Reduction in precipitation seasonality in China from 1960 to 2018

Yuna Mao[1], Guocan Wu[1], Guangzhi Xu[1], Kaicun Wang[1*]

[1] *State Key Laboratory of Earth Surface Processes and Resource Ecology, College of Global Change and Earth System Science, Beijing Normal University, Beijing, 100875, China*

Corresponding author: Kaicun Wang, kcwang@bnu.edu.cn

Early Online Release: This preliminary version has been accepted for publication in *Journal of Climate*, may be fully cited, and has been assigned DOI 10.1175/JCLI-D-21-0324.1. The final typeset copyedited article will replace the EOR at the above DOI when it is published.

ABSTRACT

Changes in precipitation seasonality or the distribution of precipitation have important impacts on hydrological extremes (e.g., floods or droughts). Precipitation extremes have been widely reported to increase with global warming; however, the variability and mechanism of precipitation seasonality have not been well quantified in China. Here, we explore the multiscale variability in precipitation seasonality from 1960 to 2018 in China. A seasonality index of precipitation is defined to quantify the precipitation seasonality with a lower value indicating a more even distribution throughout a year. The seasonality index increases from southeastern to northwestern China, with a decrease in the annual mean precipitation, a later timing of the wet season, and a shorter wet season duration. The seasonality index decreases from 1960 to 2018 in China, accompanied by the increasing duration of wet season, especially in northern climate-sensitive basins, such as the Northwest River, Hai River and Songliao River basins. Take the Northwest River basin for example, the observed significant decrease in the seasonality index (~0.02/decade) from 1960 to 2018 is consistent with a significant decrease in the ratio of annual maximum 10-day precipitation to annual precipitation, which is confirmed by their significant positive correlation (R=0.72, p=0). The El Niño–Southern Oscillation (ENSO) dominates interannual fluctuations and spatial patterns of precipitation seasonality in China. In EI Niño years, the precipitation seasonality index decreases across China except for the Yangtze River basin, with broad increases in annual precipitation.

Accepted for publication in *Journal of Climate*. DOI 10.1175/JCLI-D-21-0324.1.

KEYWORDS: Precipitation seasonality; Extreme events; ENSO; China

1. Introduction

The global water cycle has been reported to have intensified as a direct influence of global warming (Eicker et al. 2016; Huntington 2006) and is anticipated to continue under the prediction of a future warmer climate (Bengtsson 2010; Ficklin et al. 2019; Lee et al. 2018; Zhang et al. 2019b). As the key variable in the water cycle, changes in precipitation regimes have attracted widespread attention (Bhowmick et al. 2019; Chou; Lan 2012; Mardero et al. 2020; Trenberth 2011).

As one important characteristic of precipitation regimes, precipitation seasonality or the seasonal distribution of precipitation, has a large impact on the occurrence and intensity of precipitation extremes (e.g., floods or droughts) (Brönnimann et al. 2018; Konapala et al. 2020; Pendergrass; Knutti 2018; Tao et al. 2018), which exert large influences on vegetation growth (Chen et al. 2020; Dubois et al. 2014; Piao et al. 2019; Yan et al. 2016; Yun et al. 2018; Zhang et al. 2018), the planning and management of water resources (Feng et al. 2012; Hong; Kim 2011; Piao et al. 2010; Villarreal et al. 2016), and the maintenance of consistent ecosystem development (Cascante-Marín et al. 2017; Dubois et al. 2014; Peng et al. 2013; Rohr et al. 2013; Sahany et al. 2018; Zeppel et al. 2014; Zhang et al. 2019c). For example, in regimes with a high precipitation magnitude, if a region experiences strengthened seasonality, it means it is expected that a higher percentage of the annual total precipitation will occur over a few

Accepted for publication in *Journal of Climate*. DOI 10.1175/JCLI-D-21-0324.1.

very rainy days known as extreme precipitation events (e.g., floods).

In response to global climate warming, precipitation extremes have been reported to increase globally (Berg et al. 2013; Dai et al. 2020; Deng et al. 2018; Fischer; Knutti 2016; Kirchmeier-Young; Zhang 2020; Myhre et al. 2019; Papalexiou; Montanari 2019; Sun et al. 2017), while the corresponding changes in precipitation seasonality across world regions have not reached a consensus. On the one hand, some regions have experienced significant changes in precipitation seasonality, such as in the tropics (Song et al. 2018; Song et al. 2020; Song et al. 2021; Xue et al. 2013), California (Dong et al. 2019a; Dong et al. 2019b; Wang et al. 2017a), China (Tao et al. 2018), India (Sahany et al. 2018), and Mexico (Mardero et al. 2020). On the other hand, there are some results showing that precipitation seasonality has not changed, such as in the contiguous USA (Mallakpour; Villarini 2017; Pryor; Schoof 2008) and East Africa (Gebrechorkos et al. 2019). The asymmetric changes reveal the asymmetric response to global warming worldwide, and some studies have projected that precipitation seasonal distribution will be more uneven than present-day precipitation (Pascale et al. 2015b; Pendergrass; Knutti 2018) and may produce a pattern in which "seasonally variable regimes become more variable" (Konapala et al. 2020).

Precipitation extremes are also found to have increased and intensified in China (Chen et al. 2021b; Deng et al. 2018; Li et al. 2019; Liu et al. 2005; Ma et al. 2017; Sun et al. 2017; Wang et al. 2017b; Zhai et al. 2005; Zhou et al. 2016) especially in Northwest China, which has attracted much more attention to date. This is because this

Accepted for publication in *Journal of Climate*. DOI 10.1175/JCLI-D-21-0324.1.

phenomenon has been widely reported to be an exception to the "dry gets drier" paradigm and has a warming-wetting tendency (Chen et al. 2021a; Deng et al. 2014; Ge et al. 2007; Li et al. 2016; Shi et al. 2007; Tian et al. 2016; Wang et al. 2020b; Wu et al. 2019; Yao et al. 2018). One recent study shows that not only the magnitude at annual and seasonal scales is increased in this region but also the intensity and frequency of extreme precipitation are strengthened from 1961 to 2018 (Hu et al. 2021b), consistent with the reported increase in precipitation extremes (Li et al. 2019; Ma et al. 2015; Sun; Zhang 2017; Zhai et al. 2005; Zhou et al. 2016).

Progress in investigating changes in precipitation seasonality in China is very limited, and some results are not consistent in some regions. In Xinjiang province, a part of Northwest China, based on precipitation records from 55 gauge stations and a precipitation concentration index, Li et al. (2011) found that there were no significant seasonality trends from 1961 to 2008 in most parts of Xinjiang. While using a gridded precipitation datasets constructed from observed data, another study showed that Northwest China experienced a significant decrease in precipitation seasonality from 1957 to 2014 (Sun et al. 2017). Such discrepancy in long-term trends of precipitation seasonality may be possibly induced by the limited observations in northwest regions (Shen et al., 2010).

In Southeast China, with the use of the observed monthly precipitation data from 1961 to 2012, a notable increase in rainfall seasonality was detected (Deng et al. 2019). Consistent with this finding, another study found increasing seasonality over this region

Accepted for publication in *Journal of Climate*. DOI 10.1175/JCLI-D-21-0324.1.

during the period of 1960-2012 using the multi-model ensemble median value of Coupled Model Intercomparison Project Phase 5 (CMIP5) historical simulations (Deng et al. 2020). To date, there are still no specific decisions summarizing the changes in seasonality across China, and how precipitation seasonality exerts an influence on the intensity of extreme events is not well understood.

The main mechanisms behind the changes in precipitation seasonality are worth exploring to provide a better understanding of precipitation seasonality. Currently, the El Niño–Southern Oscillation (ENSO), a naturally occurring climate signal from the tropical Pacific Ocean, has been deemed the most dominant interannual signal of climate variability and has exerted a significant influence on precipitation variability in China (Dai 2021; Fatichi et al. 2012; Tian et al. 2016; Trenberth 2011; Ward et al. 2014; Zhang et al. 1999; Zhang et al. 2017). However, current studies have mostly focused on the influence of ENSO on precipitation magnitude (Dong et al. 2020; Hu et al. 2021a; Lu et al. 2019; Lv et al. 2019; Ma et al. 2018; Sun et al. 2020; Zhang et al. 2017), frequency, and intensity of rainfall events (Lv et al. 2019; Miao et al. 2019), or extreme events (Lv et al. 2019; Miao et al. 2019), and its impact on precipitation seasonality has been rarely examined in China. Good knowledge of the ENSO impact on precipitation seasonality will pave the way for predicting precipitation seasonality and forecasting possible flood/drought risks because of the predictability of ENSO with lead times of several seasons (Ward et al. 2014).

Here, to develop a better understanding of the variability and mechanism of

Accepted for publication in *Journal of Climate*. DOI 10.1175/JCLI-D-21-0324.1.

precipitation seasonality in recent decades in China, we adopt one newly proposed relative entropy method to comprehensively elucidate precipitation seasonality and its related important characteristics (annual and seasonal magnitude, timing of wet season, and duration of wet season) using daily precipitation observations from 1960 to 2018 from more than 2000 rain gauge stations. Their spatial pattern, interannual variability and long-term changes at the basin scale are explored. In addition, we investigate the possible link between precipitation seasonality and extreme events. To help explain the detected seasonality changes, we further examine the influence of the ENSO climate index and determine how this process acted by exploring large-scale atmospheric circulation anomalies.

The paper is organized as follows. Section 2 introduces the data and methods used in this study. Section 3 displays the results of precipitation climatology, spatiotemporal patterns of precipitation indices, temporal changes of precipitation extremes and the influence of the ENSO effect. In section 4, we discuss the link between precipitation seasonality and extreme events, analyze atmospheric circulation to explain the different effects of the positive and negative phases of ENSO, and conclude with a summary of the main findings and discuss the limitations of the study and future work.

2. Data and Methods

2.1 Data

The ground-based daily precipitation data from 1960 to 2018 used in this study is

Accepted for publication in *Journal of Climate*. DOI 10.1175/JCLI-D-21-0324.1.

from the China National Stations' Fundamental Elements Datasets V3.0 collected from ~2400 rain gauge stations (http://data.cma.cn). The datasets have passed rigorous quality control, such as spatiotemporal consistency checks, extreme value checks, and other procedures, and they currently serve as the latest meteorological datasets of good quality and integrity to be applied to many studies (Cao et al. 2016; Jiang et al. 2020; Xu et al. 2019). To avoid the missing values that could weaken the analysis efficiency and reliability, we apply a missing data ratio (1%) to exclude stations that have missing ~4 days for a year. The final selected 1855 stations are shown in Figure 1.

In this study, ENSO is represented by the Oceanic Niño index (ONI), which is calculated from the 3-month running mean of ERSST.v5 SST anomalies in the Niño 3.4 region (5°N-5°S, 120°-170°W) (https://origin.cpc.ncep.noaa.gov/products/analysis_monitoring/ensostuff/ONI_v5.php). The atmospheric circulation fields associated with precipitation changes, including wind fields, geopotential height, total column water vapor, and divergence of vertically integrated moisture fluxes are obtained from the latest ERA5 atmospheric reanalysis (Hersbach 2019), providing hourly estimates of a large number of atmospheric, land, and oceanic climate variables from 1950-2020 at a 0.25°×0.25° spatial resolution by combining vast amounts of historic observations into global estimates using advanced modeling and data assimilation systems. ERA5 data are spliced into two entries for 1950-1978 (preliminary back extension) and from 1979 onwards. Considering that data from 1979 onwards have assimilated from satellite data, we utilize the circulation data from 1979

Accepted for publication in *Journal of Climate*. DOI 10.1175/JCLI-D-21-0324.1.

153 to 2018 to maintain analysis efficiency.

154 *2.2 Methods*

155 2.2.1 Characterization of precipitation seasonality

156 The seasonality index is usually defined to quantify precipitation seasonality. A
157 higher seasonality index indicates a higher degree of seasonal variation in rainfall, while
158 a lower value represents a more even distribution pattern throughout a year. The
159 appearance of the seasonality index facilitates meaningful comparisons in different
160 areas (Beck et al. 2013; Fatichi et al. 2012; Fu; Wang 2019; Tan et al. 2020) and has
161 been developed in recent decades for more widespread applications (Pascale et al.
162 2015a; Xue et al. 2013). A more recent development proposed by Xue et al. (2013)
163 creatively incorporated the idea of statistical physics and information theory to obtain
164 a seasonality index by calculating the relative entropy of monthly precipitation, which
165 is independent of specific locations or arbitrary thresholds and has been used to examine
166 global seasonality characteristics and changes (Deng et al. 2019; Konapala et al. 2020;
167 Pascale et al. 2015a; Sahany et al. 2018; Tan et al. 2020). Relative entropy can measure
168 the uniformity of monthly precipitation distribution by comparing with evenly
169 distribution ($q_{m,k}$=1/12, m=1, 2, …, 12, which indicate evenly monthly distribution of
170 precipitation in each month *m* of year *k*) and provide a quantitative concentration degree
171 of precipitation, thus it is closely related to the duration of wet months. The latest study
172 showed that this method was more sensitive than other methods (Tan et al. 2020).

Accepted for publication in *Journal of Climate*. DOI 10.1175/JCLI-D-21-0324.1.

The calculation procedure for seasonality index (*SI)* in each year *k* is shown in Equations 1 and 2:

$$p_{m,k} = \frac{r_{m,k}}{r_k} \quad (1)$$

$$SI_k = \sum_{m=1}^{12} p_{m,k} \log_2 (\frac{p_{m,k}}{q_m}) \quad (2)$$

where *m* is each month (i.e., 1-12), $r_{m,k}$ is the monthly precipitation in each year *k*, and $p_{m,k}$ is the proportion of monthly precipitation accounting for annual precipitation (r_k), which indicates the monthly precipitation probability distribution. q_m is a constant of 1/12, representing uniformly distributed precipitation across 12 months. The seasonality index SI_k achieves its maximum value of $\log_2 12$ when precipitation is concentrated in a single month and is zero when precipitation is uniformly distributed among the 12 months.

Moreover, Xue et al. (2013) provided a set of statistical measures to represent three seasonality components (magnitude, timing, and duration of wet season). The magnitude is obtained by summing precipitation during a time period (e.g., year/season). The timing and duration of wet season are obtained by calculating the first and the second moments of daily precipitation time series, which indicate the centroid and spread respectively in probability and statistics theory. The centroid indicates the central tendency of daily precipitation distribution. The spread is the variance, which indicates the stability of centroid. The detailed calculation procedure is shown as follows.

The annual magnitude r_k (i.e., annual total precipitation) at each station is

Accepted for publication in *Journal of Climate*. DOI 10.1175/JCLI-D-21-0324.1.

194 calculated following Equation 3:

195 $$r_k = \sum_{d=1}^{365} r_{d,k} \quad (3)$$

196 where $r_{d,k}$ is the daily precipitation on day d of year k. This method is also used to
197 calculate the seasonal total precipitation. We define four seasons per calendar year:
198 January–March (JFM), April-June (AMJ), July–September (JAS), and October–
199 December (OND).

200 The timing of precipitation T_k in each year is obtained by computing the centroid
201 based on Equation 4:

202 $$T_k = \frac{1}{r_k}\left(\sum_{d=1}^{365} dr_{d,k}\right) \quad (4)$$

203 Based on T_k, we can obtain the duration of wet season D_k using Equation 5:

204 $$D_k = \sqrt{\frac{1}{r_k}\sum_{1}^{365} |d - T_k|^2 r_{d,k}} \quad (5)$$

205 Based on the above methods, we obtain the precipitation seasonality index,
206 annual/seasonal magnitude, and the timing and duration of the wet season for each year
207 from 1960 to 2018 in all the stations. Further, we obtain basin-scale precipitation
208 seasonality indices using spatially averaging method.

209 It should be noted that the calculation of the duration of wet season in this study
210 may produce different results compared with other methods that are not based on
211 integral properties of the rainfall distribution (Pascale et al. 2015a). For example,
212 duration based on local properties may be calculated as the retreat date minus the onset
213 date defined by a threshold (Hasson et al. 2014).

214 2.2.2 Detection of changes in precipitation seasonality indicators

Accepted for publication in *Journal of Climate*. DOI 10.1175/JCLI-D-21-0324.1.

This study uses one conventional statistic, i.e., the coefficient of variation, to study interannual variability (Fatichi et al. 2012) and Sen's slope method to detect the long-term trends of precipitation seasonality indices (Sen 1968) with a statistical significance test using a nonparametric Mann-Kendall trend test method at a significance level of 5% (Mann 1945). The coefficient of variation is a statistical measure of the dispersion of data point around the mean and is represented by the ratio between standard deviation and mean value. Sen's slope and Mann-Kendall methods are usually applied together and have been widely applied to many climate analysis studies (Basso et al. 2021; Berner et al. 2020; Perkins-Kirkpatrick; Lewis 2020; Wang et al. 2020a).

2.2.3 Characterization of precipitation extremes

To explore the link between precipitation seasonality and extremes, we further calculate annual precipitation extremes from 1960 to 2018. Considering that the definition based on the 95^{th} or 99^{th} percentile mainly focuses on the highest 5% or 1% of precipitation events(Deng et al. 2018; Li et al. 2019; Wang et al. 2017b; Zhai et al. 2005; Zhou et al. 2016), we choose another way to represent precipitation extremes by calculating the proportion of 10-day maximum precipitation in annual precipitation, which also consider moderate precipitation events. The 10-day maximum precipitation is obtained following two steps. First, daily precipitation in each year are ranked in descending order. Second, the precipitation falling on the first 10 days are summed. A higher proportion will indicate an intense tendency of precipitation extremes.

2.2.4 ENSO influences on precipitation seasonality

Given that ENSO normally matures toward the end of the year, we mainly adopt the December-January-February (DJF) Niño 3.4 value to classify ENSO years and extract time series of seasonality indices for its positive (EI Niño) and negative (La Niña) phases. To emphasize the effect of positive and negative ENSO phases, we mainly focus on strong EI Niño (ONI>1.0σ) and strong La Niña (ONI<-1.0σ) events.

To explore the ENSO effects on precipitation seasonality indices, we use two widely used methods, i.e., correlation analysis and composite analysis (Jong et al. 2016; Lu et al. 2019; Miao et al. 2019). We first detrend the time series of seasonality indices before performing the analysis. For correlation analysis, we calculate the correlation coefficient (R) between the annual ONI value and the precipitation seasonality indices using the Pearson correlation method, with a range of -1 to 1. A higher positive R represents high positive teleconnection and Student's t-test is used to test the significance of the correlation.

Composite analysis is a standard method used to reflect the possible influence of atmospheric circulation anomalies on climate variables by calculating the difference between EI Niño/La Niña and neutral years (Davey et al. 2014; Lv et al. 2019; Shin; Park 2020; Welhouse et al. 2016; Xie et al. 2017). To test whether such a difference is statistically significant, we use a nonparametric Mann-Whitney U-test method, which does not require that the two datasets under comparison have the same sizes or normal distributions (Corder; Foreman 2009; Teegavarapu et al. 2013).

3. Results

3.1 Representation of precipitation seasonality

Based on the introduced methods, we obtain the timing, duration of wet season, and seasonality index in China and its nine major river basins during the period of 1960-2018. Figure 2 provides the intuitive representation of precipitation seasonality characteristics in each basin by displaying daily and monthly precipitation time series. To better present seasonal differences among basins, we calculate the proportion of daily and monthly precipitation in the annual mean precipitation in each basin. Generally, the seasonal characteristics in all the regions display a unimodal pattern, i.e., peak precipitation is concentrated in one month (June or July).

Six basins, including the Hai River, Songliao River, Yellow River, Huai River, and Northwest River basins, which are mainly distributed in northern China, have a sharp peak that start from ~June and end in ~August, accompanied by a later timing, shorter duration of wet season, and higher seasonality index. For example, precipitation in the Hai River basin displays a steepest peak with precipitation in July accounting for almost 30% of the annual total precipitation, thus has the highest seasonality index value of 0.78. Three basins, including the Pearl River, Southeast river, and Yangtze River in southern China, have flat peaks that start earlier in May and reveal an even monthly distribution. Overall, as China a whole, the seasonal distribution pattern is similar to that in southern China, while the peak month of precipitation is the same as that in northern China.

Accepted for publication in *Journal of Climate*. DOI 10.1175/JCLI-D-21-0324.1.

3.2 Spatial pattern of precipitation seasonality

We further obtain the spatial pattern of the annual mean precipitation seasonality index and three other seasonality indicators, including the annual magnitude, the timing, and the duration of the wet season at each gauge station (Figure 3). Figure 3a indicates the spatial distribution of the annual mean precipitation with a range of ~100-1800 mm and a decrease from southeast to northwest, which is consistent with China's climate regionalization and humid-arid distribution (Zheng et al. 2013).

Figure 3b shows the regionally varying mean concentration date of the wet season ranging from June to August. The wet season starts in the south and moves north as the months progress. Timing in southern China starts earlier from June-July, and begins in northern China in July-August. Not only do different basins display high variation, but one basin can also experience significant differences, e.g., three kinds of timing exist in the Yangtze River basin, featuring the earliest date in June in the downstream and the latest date in August in the upstream. The stepwise migration of wet months from south to north has been demonstrated to be highly correlated with the onset and movement of the East Asian summer monsoon, which is primarily affected by the Western Pacific subtropical high (Ding et al. 2020; Fu et al. 2008; Huang et al. 2018; Lu et al. 2016). In Figure 3c, the duration of the wet season in China ranges from ~1.5 month to 3 months from northwest to southeast. The longer duration (> 3 months) mainly appears in the southeast, middle and down streams of the Yangtze River, and north of the Northwest River basins. The shorter duration (~1.5 month) is found in Songliao and Hai River

Accepted for publication in *Journal of Climate*. DOI 10.1175/JCLI-D-21-0324.1.

298 basins. The spatial patterns of timing and duration of wet season displays high
299 consistence. For example, the earlier timing corresponds to a longer duration of wet
300 season in south east river basins. The seasonality index map is shown in Figure 3d,
301 which has a similar distribution with timing and duration. From the southeast to
302 northwest, the seasonality index of precipitation increases from ~0.2 to ~1. The stations
303 with a lower seasonality index are generally distributed in the regions with a longer
304 duration and an earlier timing of wet season.

305 Further analysis of the mean seasonal precipitation distribution is shown in Figure
306 S1. Although the annual total precipitation displays smooth transitions from the
307 southern to northern regions, their seasonal distribution indicates remarkable
308 differences, which reveal high heterogeneity in the annual rainfall distribution. In
309 northern river basins, such as the Songliao, Hai River, Yellow River, Northwest River,
310 and northern Huai River basins, the precipitation amounts in the July-September
311 (~summer) season account for more than half of the annual precipitation, followed by
312 that in the April-June season (~30%), the October-December season (10%) and the
313 January-March season (<5%). In southern river basins, such as the Pearl River,
314 Southeast River, and middle and downstream of the Yangtze River basin, the April-
315 June season account for half, followed by July-September (30%), January-March (20%),
316 and October-December (10%). Overall, precipitation in China represents a strong
317 seasonal pattern and is mainly concentrated in the April-June (~spring) and July-
318 September (~summer) seasons, also known as the wet season (April-September) (Fan

Accepted for publication in *Journal of Climate*. DOI 10.1175/JCLI-D-21-0324.1.

et al. 2018).

Overall, in southern China, including the Pearl River, Southeast River, and middle and downstream of the Yangtze River basin in the subtropical monsoon zone, the seasonality index is lower, accompanied by a larger annual mean precipitation mainly concentrated in the April-June season, an earlier concentration date, and a longer duration of the wet season. In contrast, the northern China, specifically the western Songliao River, northern Hai River, Yellow River, upstream of Yangtze and southern Southwest River basin in arid regions, is characterized by a higher seasonality index and a lower precipitation magnitude mainly concentrated in the July-September season, a later concentration date and a shorter duration of the wet season. Figure 3b and 3c can be combined to partly explain the seasonality index map shown in Figure 3d.

In addition to the distinct seasonality differences represented in the northern and southern China, there are notable divisions within river basins, such as the apparently different patterns in the northern and southern parts of the Northwest River basin and the western and eastern parts of the Songliao River basin. In the Northwest River basin, although the total annual rainfall in the subregions is similar, the timing, duration, and seasonality index present opposite directions compared with that in the northern and southern parts. The seasonality index is larger in regions where the duration of the wet season is shorter, which is consistent with the results of a previous study (Li et al. 2011). The division in the Northwest River basin could be caused by the uplift of the Tian

Accepted for publication in *Journal of Climate*. DOI 10.1175/JCLI-D-21-0324.1.

Shan Mountains and Pamir Plateau, which influences the water vapor transport paths (Sha et al. 2018). In the Songliao River basin, the western part is characterized by shorter duration and a stronger seasonality index, while the opposite is found in the eastern part. This phenomenon can be explained by the U-shaped topography due to the Changbai Mountains that block water vapor from southwesterly winds (Liang et al. 2011; Liu et al. 2017).

3.3 Interannual variability and long-term changes in precipitation seasonality

Interannual variability represented by the coefficient of variation of seasonality indicators during the period of 1960-2018 is shown in Figure 4. We find that the seasonality index has higher interannual variability than the other three indicators. The higher interannual variability (coefficient of variation >0.3) is mainly observed in the Northwest River, southern Huai River, downstream of the Yangtze River, Southeast, and part of the Pearl River basins. In the Northwest River basin, all seasonality indicators display higher coefficients of variation than those in the other regions, implying a higher "year-to-year" variation that is sensitive to interannual climate changes. However, the timing of the wet season indicates no obvious change during the past 59 years.

The interannual variation and long-term trends of precipitation seasonality time series from 1960 to 2018 in China (Figure 5) and its nine river basins (Figures 6-9, and Figure S2) are also calculated. The interannual variation of timing, duration of wet season and seasonality index in the nine basins are shown in Figures 6-8 and magnitude

Accepted for publication in *Journal of Climate*. DOI 10.1175/JCLI-D-21-0324.1.

361 at annual and seasonal scales are shown in Figure S2. All the calculated long-term
362 trends are summarized in Figure 9(e). For China as a whole, Figure 5a indicates that
363 the annual precipitation amount is mainly determined by precipitation fluctuation in
364 April-June and July-September seasons and displays a weak increasing trend, which is
365 the combined result of decreased precipitation in July-September season and increased
366 precipitation in the other three seasons (Figure 9). The annual timing in China comes
367 earlier, the duration is significantly prolonged, and the seasonality index is obviously
368 decreased, implying a more even precipitation distribution from 1960 to 2018.

369 Besides Southwest River basin, interannual variation of precipitation magnitude
370 in most northern river basins such as Hai River basin, Songliao River basin, Yellow
371 River basin, and Huai River basin are mainly determined by precipitation fluctuation in
372 July-September, while in Pearl River basin, Yangtze River basin, and Southeast River
373 basin, precipitation in April-June plays a more important role in interannual variation.
374 Regarding the annual precipitation time series from 1960 to 2018, Figure S2 and Figure
375 9 show that most northern river basins, including the Hai River, Songliao River, Yellow
376 River, Huai River, and Southwest River, indicate weak decreasing trends, while the
377 Northwest and southern river basins, including the Yangtze River, Pearl River, and
378 Southeast River, display increasing trends, consistent with the previous findings in
379 many researches ((Day et al. 2018; Li et al. 2016; Li et al. 2018; Nigam et al. 2015a;
380 Wu et al. 2019).

381 Figures 6-9 also shows that some river basins, such as the Northwest, Hai River,

Accepted for publication in *Journal of Climate*. DOI 10.1175/JCLI-D-21-0324.1.

382 and Songliao River, indeed experience statistically significant changes in precipitation
383 seasonality in the past 60 years in China. In the Songliao River basin as shown in Figure
384 S2 and 9e, although no obvious changes in annual magnitude are observed, the seasonal
385 precipitation (i.e., January-March, April-June, and July-September) experience
386 significant changes. The significant increases in the January-March and April-June
387 seasons are counterbalanced by a remarkable decrease in the July-September season,
388 contributing to the insignificant decrease in the annual amount. In addition, the timing
389 is significantly advanced (Figure 6b) and the duration is significantly increased (Figure
390 7b), accompanied with a significantly decreased seasonality index (Figure 8b). Similar
391 changes are also observed in the most river basins, especially notable in the Hai River
392 and Northwest River basins. The Northwest River basin experiences a significant
393 decrease of seasonality index ~0.02 per decade (Figure 8f and figure 9e). Considering
394 the uneven and limited distribution of gauge stations in the Northwest River basin, the
395 significant decrease of seasonality index mainly represents the changes in northern part.
396 Figure 8 and Figure 9e also reveal that the seasonality index across China represents a
397 negative trend, indicating a more evenly distributed precipitation in past years. The
398 same analysis for each gauge station shown in Figure 9(a-d) shows similar changes.

399 ### *3.4 long-term changes in precipitation extremes*

400 The time series of precipitation extremes characterized by the top 10-day
401 maximum precipitation proportion are shown in Figure 10. In the northern river basins,
402 including the Hai River, Songliao River, Yellow River, Huai River, and Northwest River,

Accepted for publication in *Journal of Climate*. DOI 10.1175/JCLI-D-21-0324.1.

precipitation extremes account for more than half of annual precipitation amount. For example, precipitation extremes have a proportion of ~65% in the Northwest River basin. While in the southern river basins including Yangtze River, Pearl River, and Southeast River, precipitation extremes account for ~40% of annual precipitation amount. The inconsistent proportions between northern and southern China imply that precipitation extremes in the northern China are more intense than those in the southern China.

From Figure 10, we also find that precipitation extremes in the Northwest River basin observes significant decreasing trends of -0.05 per year (p=0) and indicate high consistence with the downward tendency of seasonality index from 1960 to 2018. Though no obvious changes of precipitation extremes are detected in the other river basins, the annual proportion of 10-day maximum precipitation and annual seasonality index have high consistency, which means that the interannual variability of the 10-day maximum precipitation is may highly dependent on the precipitation seasonality. This dependence is further demonstrated by their significant and positive correlation coefficient. The range of the correlation coefficient is ~0.4-0.7 (p=0), with the highest value shown in the Northwest River basin. The analysis based on the 5-day maximum precipitation also produce almost the same results (Figure S3). Therefore, the reduced precipitation seasonality corresponds to the decreasing precipitation extremes characterized by the 10-day/5-day maximum precipitation across China.

Accepted for publication in *Journal of Climate*. DOI 10.1175/JCLI-D-21-0324.1.

3.5 *Influence of ENSO and its related circulation on precipitation seasonality in China*

To investigate the ENSO effect, we first calculate the correlation coefficient (R) between the Niño-3.4 index and the seasonality indices from 1960 to 2018 in China and nine river basins, as shown in Figure 11. ENSO has significantly influenced precipitation seasonality indices in China. Generally, the Niño-3.4 index has a strong positive correlation with precipitation magnitude in China (R=0.4, p=0.01), whereas its relationship with the other three seasonality indices are complicated. In nine river basins, the correlation analysis shows that ENSO has significant negative and positive correlations with precipitation seasonality index in the Northwest River and Yangtze River basins respectively. Generally, ENSO displays a strong negative correlation with timing of wet season across China.

To distinguish the different roles of the positive and negative phases of ENSO on precipitation seasonality indices, we further calculate the composite difference (i.e., EI Niño-La Niña) shown in Figure 12. The figures show that ENSO can indeed bring about notable differences in precipitation seasonality indices. In EI Niño years, the annual precipitation throughout China displays significant increases, and timing of wet season comes earlier. While the other two seasonality indices show large spatial heterogeneity with duration and seasonality index usually indicating opposite changes. In the northwest part of the Northwest River basin, Songliao River, Yellow River, and Yangtze River basins, durations significantly decrease and seasonality indexes increase. In contrast, in Hai River, Huai River, Southeast River, and Pearl

Accepted for publication in *Journal of Climate*. DOI 10.1175/JCLI-D-21-0324.1.

River basins close to the Pacific Ocean, durations increases and seasonality indexes decrease.

Further we examine monthly atmospheric circulation anomaly induced from EI Niño and La Niña phases with ERA5 datasets from 1979 to 2018, focusing on the atmospheric water vapor transport using the column water vapor flux integrated from the surface to the top of the atmosphere and the corresponding water vapor flux divergence. From Figure 13 and 14, we find that total column water vapor in eastern China in EI Niño years are higher and moisture convergence (negative divergence values indicate moisture convergence) appears in most months, which shows an even water vapor distribution and indicate a lower precipitation seasonality. In contrast, the water vapor shows high concentration that induces a high seasonality index in La Niña years.

4. Discussion and Conclusions

Using gauge-based daily precipitation records from 1960 to 2018 from 1855 stations, the research studies the variability and mechanism of precipitation seasonality in China. The precipitation climatology, spatial pattern, interannual variability and long-term trends of precipitation seasonality (seasonality index) and related characteristics (annual and seasonal magnitude, timing, and duration of wet season) are shown for nine major river basins in China. The long-term changes of precipitation extremes are detected and the link with seasonality index are explored. Furthermore, the role of ENSO in changing precipitation seasonality is investigated.

Accepted for publication in *Journal of Climate*. DOI 10.1175/JCLI-D-21-0324.1.

From southeastern to northwestern China, precipitation seasonality characterized by a seasonality index increases, accompanied by a decrease in the annual mean precipitation, a later timing of the wet season, and a shorter wet season duration. From 1960 to 2018, precipitation seasonality displays large interannual variability and shows considerable changes. Larger interannual variability mainly appear in the northwest and southeast river basins. The seasonality index has been widely reduced across China, especially in northern climate-sensitive basins (i.e., the Northwest River, Hai River, and Songliao River basins), with a significant decrease of ~0.02 per decade (p=0). The reduced seasonality index is accompanied by a prolonged duration of the wet season.

The widely reduced seasonality index observed in this study indicates a more even rainfall distribution throughout a year, which implies fewer precipitation extremes in the past 60 years. This finding seems to be in contrast to the reported increasing extreme precipitation events across China, which are usually defined by the 95^{th} percentile of precipitation on rainy days (Deng et al. 2018; Li et al. 2019; Wang et al. 2017b; Zhai et al. 2005; Zhou et al. 2016) or 99^{th} wet-day percentile (Contractor et al. 2021). Considering that the definition based on the 95^{th} or 99^{th} percentile mainly focuses on the highest 5% or 1% of precipitation events, we choose another way to represent precipitation extremes by calculating the proportion of 5/10-day maximum precipitation in annual precipitation, which also consider moderate precipitation events. We find that the annual proportion of 5/10-day maximum precipitation and annual seasonality index have high consistency, which means that the reduced precipitation

Accepted for publication in *Journal of Climate*. DOI 10.1175/JCLI-D-21-0324.1.

seasonality corresponds to the decreasing precipitation extremes characterized by the 10-day/5-day maximum precipitation across China and does not contradict the increasing trend of precipitation extremes characterized by the 95th percentile precipitation of rainy days. The widely declined seasonality index in China indicate a more even precipitation distribution through a year, which is more efficient for vegetation growth compared with precipitation extreme events.

In addition to the remarkable changes in the seasonality index, this study investigates the associated changes in precipitation magnitude. The detected magnitude changes in this study agree well with the climate change regionalization in China from 1961 to 2010 documented by Shi et al. (2014), characterized by wetting-northwest and southeast and drying-southwest river basins. The changes in precipitation magnitude are found to be related to many factors, such as increased aerosol and dust loadings (Bollasina et al. 2011; Li et al. 2018; Wu et al. 2016; Yu et al. 2016), significant land-use land-cover change (Bollasina; Nigam 2011), and increased greenhouse gas emissions (Tian et al. 2018), SST variability (Nigam et al. 2015b), interdecadal variability in the EASM (Ding et al. 2018) or changes in the frequency of frontal rain events (Day et al. 2018). Our study provides another possibility that the changes in seasonality may influence the changing the precipitation magnitude in China.

We also find that the Northwest River basin has experienced the most distinct decreasing trend in precipitation seasonality compared with the other basins. The significant decrease in the seasonality index is accompanied by a significant longer

Accepted for publication in *Journal of Climate*. DOI 10.1175/JCLI-D-21-0324.1.

duration of wet season, and a significant increase in magnitude. The Northwest River basin located in an arid climate region observes a significant increase in annual precipitation (Qian; Lin 2005; Shi et al. 2007; Yang Jianping 2002). Our study further shows that the observed decreased seasonality in this region may contribute to the increased magnitude by producing a more even distribution of precipitation with an increase of annual total amount.

Many studies have explored the drivers behind the wetting phenomenon in the Northwest River basin. In this basin, precipitation is mainly concentrated in summer as a result of the water transport by westerlies wind (Chen et al. 2019; Zhang et al. 2019a); thus, most studies have focused on investigating the water transport sources in summer. Li et al. (2016) suggests that the strengthening of the Western Pacific subtropical high and the North American subtropical high are likely to be the main cause. Wu et al. (2019) attributed the increased precipitation to the changing recycling precipitation contributed by local evapotranspiration and changing precipitation contributed by advection moisture. The latest study by Chen et al. (2021a) showed that the weakening of the EASM that is accompanied by a persistent westward shift of the Western Pacific subtropical high and an increasing frequency of Mongolian anticyclone activities has directly influenced the amount of summer precipitation.

However, these studies deem that the precipitation variation in summer precipitation plays the most important role in yearly changes in the Northwest River basin (Li et al. 2016). Our study finds that the increase in annual precipitation could be

Accepted for publication in *Journal of Climate*. DOI 10.1175/JCLI-D-21-0324.1.

the combined result of a significant increase from all seasons from 1960-2018 (Figure S1 and Figure 9). Therefore, in addition to the focus on summer precipitation anomalies, the atmospheric circulation anomalies induced by climate regimes in other seasons should be considered in future studies.

To better understand the changes in precipitation seasonality, we explore the ENSO effect on changing precipitation seasonality. Both correlation analysis and composite analysis results affirm the important role of ENSO in governing interannual fluctuations in seasonality. In EI Niño years, annual precipitation amounts significantly increase and timings of wet season are significantly advanced. The seasonality index decreases in eastern China close to the Pacific Ocean, and mainly increases in the Songliao River basin, southern part of Yellow River basin and the Yangtze River basin, which could be explained by the changes in the duration of the wet season. In the regions with a decreasing seasonality, the duration length is prolonged. ENSO produces increasing annual precipitation amounts throughout the above regions, which means that precipitation seasonality may exert different impacts on annual precipitation in different regions.

In conclusion, our study shows that precipitation seasonality decreases from 1960 to 2018 in China, especially in northern climate-sensitive basins. In the Northwest River basin, the observed significant decrease (~0.02/decade) is consistent with a significant decrease in the proportion of the annual maximum 10-day precipitation in annual precipitation, revealed by their highly and significant correlation. This finding is not in

Accepted for publication in *Journal of Climate*. DOI 10.1175/JCLI-D-21-0324.1.

549 contrast to the reports of increasing precipitation extremes, which mainly focused on
550 the highest 1% or 5% precipitation events. The reduced seasonality index induces a
551 more even distribution, and the 10-day maximum precipitation considers more
552 moderate precipitation events, which may balance the effect of the highest precipitation
553 events. Atmospheric circulation anomalies from ENSO have been found to exert
554 important impacts on changes in precipitation seasonality.

555 It should be noted that besides ENSO, there are several factors including other
556 global climate indices (e.g., North Atlantic Oscillation (NAO), Pacific Decadal
557 Oscillation (PDO), Atlantic Multidecadal Oscillation (AMO)) and anthropogenic
558 activities influencing precipitation seasonality changes, and the detailed physical
559 processes are complicated. NAO, PDO and AMO have been found to be significantly
560 correlated with precipitation seasonality, especially in monsoon regions of China,
561 where significant positive or negative seasonality anomalies are detected during
562 positive or negative phases(Deng et al. 2019). The increasing pattern of anthropogenic
563 aerosols in eastern China is found to be consistent with the enhancement of large-scale
564 precipitation for the period of 1952-2015(Yu et al. 2016), considering the anthropogenic
565 aerosols are seasonally dependent (e.g., winter maximum-summer minimum of
566 anthropogenic sulfate aerosol in the southern China)(Wang et al. 2003), precipitation
567 seasonality may also be changed. Based on historical simulations of CMIP5 general
568 circulation models from 1960 to 2012, a recent study discovered that anthropogenic
569 forcing enhances precipitation seasonality over many parts of global monsoon

Accepted for publication in *Journal of Climate*. DOI 10.1175/JCLI-D-21-0324.1.

570 regions(Deng et al. 2020). Here, we focus only on the induced impact from the
571 dominant factor, i.e., ENSO. In future studies, we should combine ENSO with other
572 important climate indices to quantitatively compute their individual contributions to
573 precipitation seasonality changes. In addition, we find that although precipitation
574 seasonality is positively correlated with precipitation extremes characterized by the 10-
575 day/5-day precipitation amounts across China, the influence on the average
576 precipitation amount at the annual scale may be different in different regions and needs
577 to be further explored. We also find that the wetting phenomenon in the Northwest
578 River basin should be the combined increase across all four seasons, while current
579 studies have mainly focused on the increase in summer. The reasons accounting for the
580 increasing precipitation in other seasons should also be investigated in the future. It
581 should be noted that considering the uneven and limited gauge stations in Northwest
582 and Southwest River basins, the results in investigation precipitation seasonality
583 changes in this study may be biased and further uncertainty analysis are needed in the
584 future work.

585 *Acknowledgments*

586 This research is funded by the National Natural Science Foundation of China (No.
587 42005127). This research is also funded by the National Basic Research Program of
588 China (No. 2020YFA0608201), the Fundamental Research Funds for the Central
589 Universities, the National Basic Research Program of China (No. 2017YFA0603601)
590 and the National Natural Science Foundation of China (No. 41930970 and 41525018).

591 REFERENCES

592 Basso, B., R. A. Martinez-Feria, L. Rill, and J. T. Ritchie, 2021: Contrasting long-
593 term temperature trends reveal minor changes in projected potential evapotranspiration
594 in the US Midwest. *Nat. Commun.*, **12,** 1476, http://doi.org/10.1038/s41467-021-
595 21763-7.

596 Beck, H. E., A. I. J. M. van Dijk, D. G. Miralles, R. A. M. de Jeu, L. A. Bruijnzeel,
597 T. R. McVicar, and J. Schellekens, 2013: Global patterns in base flow index and
598 recession based on streamflow observations from 3394 catchments. *Water Resour. Res.*,
599 **49,** 7843-7863, http://doi.org/https://doi.org/10.1002/2013WR013918.

600 Bengtsson, L., 2010: The global atmospheric water cycle. *Environ. Res. Lett.*, **5,**
601 025202, http://doi.org/10.1088/1748-9326/5/2/025202.

602 Berg, P., C. Moseley, and J. O. Haerter, 2013: Strong increase in convective
603 precipitation in response to higher temperatures. *Nat. Geosci.*, **6,** 181-185,
604 http://doi.org/10.1038/ngeo1731.

605 Berner, L. T., and Coauthors, 2020: Summer warming explains widespread but not
606 uniform greening in the Arctic tundra biome. *Nat. Commun.*, **11,** 4621,
607 http://doi.org/10.1038/s41467-020-18479-5.

608 Bhowmick, M., S. Sahany, and S. K. Mishra, 2019: Projected precipitation
609 changes over the south Asian region for every 0.5 °C increase in global warming.
610 *Environ. Res. Lett.*, **14,** 054005, http://doi.org/10.1088/1748-9326/ab1271.

611 Bollasina, M., and S. Nigam, 2011: Modeling of Regional Hydroclimate Change

Accepted for publication in *Journal of Climate*. DOI 10.1175/JCLI-D-21-0324.1.

over the Indian Subcontinent: Impact of the Expanding Thar Desert. *J. Clim.*, **24,** 3089-3106, http://doi.org/10.1175/2010JCLI3851.1.

Bollasina, M. A., Y. Ming, and V. Ramaswamy, 2011: Anthropogenic aerosols and the weakening of the South Asian summer monsoon. *Science*, **334,** 502-505, http://doi.org/10.1126/science.1204994.

Brönnimann, S., J. Rajczak, E. M. Fischer, C. C. Raible, M. Rohrer, and C. Schär, 2018: Changing seasonality of moderate and extreme precipitation events in the Alps. *Nat. Hazards Earth Syst. Sci.*, **18,** 2047-2056, http://doi.org/10.5194/nhess-18-2047-2018.

Cao, L., Y. Zhu, G. Tang, F. Yuan, and Z. Yan, 2016: Climatic warming in China according to a homogenized data set from 2419 stations. *Int. J. Climatol.*, **36,** 4384-4392, http://doi.org/https://doi.org/10.1002/joc.4639.

Cascante-Marín, A., C. Trejos, and R. Alvarado, 2017: Association between rainfall seasonality and the flowering of epiphytic plants in a Neotropical montane forest. *Biotropica*, **49,** 912-920, http://doi.org/10.1111/btp.12478.

Chen, C., X. Zhang, H. Lu, L. Jin, Y. Du, and F. Chen, 2021a: Increasing summer precipitation in arid Central Asia linked to the weakening of the East Asian summer monsoon in the recent decades. *Int. J. Climatol.*, **41,** 1024-1038, http://doi.org/https://doi.org/10.1002/joc.6727.

Chen, F., and Coauthors, 2019: Westerlies Asia and monsoonal Asia: Spatiotemporal differences in climate change and possible mechanisms on decadal to

Accepted for publication in *Journal of Climate*. DOI 10.1175/JCLI-D-21-0324.1.

633 sub-orbital timescales. *Earth-Sci. Rev.*, **192,** 337-354,
634 http://doi.org/https://doi.org/10.1016/j.earscirev.2019.03.005.
635 Chen, Y., W. Li, X. Jiang, P. Zhai, and Y. Luo, 2021b: Detectable Intensification
636 of Hourly and Daily Scale Precipitation Extremes across Eastern China. *J. Clim.*, **34,**
637 1185-1201, http://doi.org/10.1175/JCLI-D-20-0462.1.
638 Chen, Z., W. Wang, and J. Fu, 2020: Vegetation response to precipitation
639 anomalies under different climatic and biogeographical conditions in China. *Sci. Rep.*,
640 **10,** 830, http://doi.org/10.1038/s41598-020-57910-1.
641 Chou, C., and C.-W. Lan, 2012: Changes in the Annual Range of Precipitation
642 under Global Warming. *J. Clim.*, **25,** 222-235, http://doi.org/10.1175/JCLI-D-11-
643 00097.1.
644 Contractor, S., M. G. Donat, and L. V. Alexander, 2021: Changes in Observed
645 Daily Precipitation over Global Land Areas since 1950. *J. Clim.*, **34,** 3-19,
646 http://doi.org/10.1175/JCLI-D-19-0965.1.
647 Corder, G. W., and D. I. Foreman, 2009: Comparing Two Unrelated Samples: The
648 Mann–Whitney U-Test. *Nonparametric Statistics for Non-Statisticians*, 57-78.
649 Dai, A., 2021: Hydroclimatic trends during 1950–2018 over global land. *Clim.*
650 *Dyn.*, http://doi.org/10.1007/s00382-021-05684-1.
651 Dai, A., R. M. Rasmussen, C. Liu, K. Ikeda, and A. F. Prein, 2020: A new
652 mechanism for warm-season precipitation response to globalwarming based on
653 convection-permitting simulations. *Clim. Dyn.*, **55,** 343-368,

Accepted for publication in *Journal of Climate*. DOI 10.1175/JCLI-D-21-0324.1.

http://doi.org/10.1007/s00382-017-3787-6.

Davey, M. K., A. Brookshaw, and S. Ineson, 2014: The probability of the impact of ENSO on precipitation and near-surface temperature. *Clim. Risk Manage.*, **1,** 5-24, http://doi.org/https://doi.org/10.1016/j.crm.2013.12.002.

Day, J. A., I. Fung, and W. Liu, 2018: Changing character of rainfall in eastern China, 1951–2007. *Proc. Natl. Acad. Sci. U.S.A.*, **115,** 2016, http://doi.org/10.1073/pnas.1715386115.

Deng, H., Y. Chen, X. Shi, W. Li, H. Wang, S. Zhang, and G. Fang, 2014: Dynamics of temperature and precipitation extremes and their spatial variation in the arid region of northwest China. *Atmos. Res.*, **138,** 346-355, http://doi.org/https://doi.org/10.1016/j.atmosres.2013.12.001.

Deng, S., C. Sheng, N. Yang, L. Song, and Q. Huang, 2020: Anthropogenic forcing enhances rainfall seasonality in global land monsoon regions. *Environ. Res. Lett.*, **15,** 104057, http://doi.org/10.1088/1748-9326/abafd3.

Deng, S., and Coauthors, 2019: Rainfall seasonality changes and its possible teleconnections with global climate events in China. *Clim. Dyn.*, **53,** 3529-3546, http://doi.org/10.1007/s00382-019-04722-3.

Deng, Y., W. Jiang, B. He, Z. Chen, and K. Jia, 2018: Change in Intensity and Frequency of Extreme Precipitation and its Possible Teleconnection With Large-Scale Climate Index Over the China From 1960 to 2015. *J. Geophys. Res.: Atmos.*, **123,** 2068-2081, http://doi.org/https://doi.org/10.1002/2017JD027078.

675 Ding, X., L. Zheng, X. Zheng, and S.-J. Kao, 2020: Holocene East Asian Summer
676 Monsoon Rainfall Variability in Taiwan. *Front. Earth Sci.*, **8**,
677 http://doi.org/10.3389/feart.2020.00234.
678 Ding, Y., D. Si, Y. Liu, Z. Wang, Y. Liu, L. Zhao, and Y. Song, 2018: On the
679 characteristics, driving forces and inter-decadal variability of the East Asian summer
680 monsoon. *Chinese Journal of Atmospheric Sciences*, **42,** 533-558,
681 http://doi.org/10.3878/j.issn.1006-9895.1712.17261.
682 Dong, L., L. R. Leung, J. Lu, and Y. Gao, 2019a: Contributions of Extreme and
683 Non-Extreme Precipitation to California Precipitation Seasonality Changes Under
684 Warming. *Geophys. Res. Lett.*, **n/a**, http://doi.org/10.1029/2019GL084225.
685 Dong, L., L. Leung, J. Lu, and F. Song, 2019b: Mechanisms for an Amplified
686 Precipitation Seasonal Cycle in the U.S. West Coast under Global Warming. *J. Clim.*,
687 **32**, http://doi.org/10.1175/JCLI-D-19-0093.1.
688 Dong, Y., and Coauthors, 2020: Teleconnection patterns of precipitation in the
689 Three-River Headwaters region, China. *Environ. Res. Lett.*, **15,** 104050,
690 http://doi.org/10.1088/1748-9326/aba8c0.
691 Dubois, N., and Coauthors, 2014: Indonesian vegetation response to changes in
692 rainfall seasonality over the past 25,000 years. *Nat. Geosci.*, **7,** 513-517,
693 http://doi.org/10.1038/ngeo2182.
694 Eicker, A., E. Forootan, A. Springer, L. Longuevergne, and J. Kusche, 2016: Does
695 GRACE see the terrestrial water cycle 'intensifying'? *J. Geophys. Res.: Atmos.*, **121,**

733-745, http://doi.org/10.1002/2015jd023808.

Fan, Q., A. Zhao, A. Zhang, L. Feng, Y. Zhao, and H. Liu, 2018: Analysis of Spatiotemporal Characteristics of Drought and Flood in the Haihe River Basin from 1965 to 2015. *International Conference on Geo-informatics in Sustainable Ecosystem and Society*.

Fatichi, S., V. Y. Ivanov, and E. Caporali, 2012: Investigating Interannual Variability of Precipitation at the Global Scale: Is There a Connection with Seasonality? *J. Clim.*, **25,** 5512-5523, http://doi.org/10.1175/JCLI-D-11-00356.1.

Feng, X., G. Vico, and A. Porporato, 2012: On the effects of seasonality on soil water balance and plant growth. *Water Resour. Res.*, **48**, http://doi.org/10.1029/2011WR011263.

Ficklin, D. L., J. T. Abatzoglou, and K. A. Novick, 2019: A New Perspective on Terrestrial Hydrologic Intensity That Incorporates Atmospheric Water Demand. *Geophys. Res. Lett.*, **46,** 8114-8124, http://doi.org/10.1029/2019GL084015.

Fischer, E. M., and R. Knutti, 2016: Observed heavy precipitation increase confirms theory and early models. *Nat. Clim. Change*, **6,** 986-991, http://doi.org/10.1038/nclimate3110.

Fu, C., Z. Jiang, Z. Guan, J. He, and Z. Xu, 2008: Climate of China and East Asian Monsoon. *Regional Climate Studies of China*, C. Fu, Z. Jiang, Z. Guan, J. He, and Z. Xu, Eds., Springer Berlin Heidelberg, 1-48.

Fu, J., and W. Wang, 2019: On the lower bound of Budyko curve: The influence

Accepted for publication in *Journal of Climate*. DOI 10.1175/JCLI-D-21-0324.1.

of precipitation seasonality. *J. Hydrol.*, **570,** 292-303, http://doi.org/https://doi.org/10.1016/j.jhydrol.2018.12.062.

Ge, Q., S. Wang, X. Wen, C. Shen, and Z. Hao, 2007: Temperature and precipitation changes in China during the Holocene. *Adv. Atmos. Sci.*, **24,** 1024-1036, http://doi.org/10.1007/s00376-007-1024-7.

Gebrechorkos, S. H., S. Hülsmann, and C. Bernhofer, 2019: Long-term trends in rainfall and temperature using high-resolution climate datasets in East Africa. *Sci. Rep.*, **9,** 11376, http://doi.org/10.1038/s41598-019-47933-8.

Hasson, S., V. Lucarini, S. Pascale, and J. Böhner, 2014: Seasonality of the hydrological cycle in major South and Southeast Asian river basins as simulated by PCMDI/CMIP3 experiments. *Earth Syst. Dynam.*, **5,** 67-87, http://doi.org/10.5194/esd-5-67-2014.

Hersbach, H., Bell, B., Berrisford, P., Biavati, G., Horányi, A., Muñoz Sabater, J., Nicolas, J., Peubey, C., Radu, R., Rozum, I., Schepers, D., Simmons, A., Soci, C., Dee, D., 2019: ERA5 monthly averaged data on pressure levels from 1979 to present. *Copernicus Climate Change Service (C3S) Climate Data Store (CDS)*, http://doi.org/10.24381/cds.6860a573.

Hong, J., and J. Kim, 2011: Impact of the Asian monsoon climate on ecosystem carbon and water exchanges: a wavelet analysis and its ecosystem modeling implications. *Global Change Biol.*, **17,** 1900-1916, http://doi.org/10.1111/j.1365-2486.2010.02337.x.

Accepted for publication in *Journal of Climate*. DOI 10.1175/JCLI-D-21-0324.1.

738 Hu, S., T. Zhou, and B. Wu, 2021a: Impact of Developing ENSO on Tibetan
739 Plateau Summer Rainfall. *J. Clim.*, **34,** 3385-3400, http://doi.org/10.1175/JCLI-D-20-
740 0612.1.

741 Hu, W., J. Yao, Q. He, and J. Chen, 2021b: Changes in precipitation amounts and
742 extremes across Xinjiang (northwest China) and their connection to climate indices.
743 *PeerJ*, **9,** e10792, http://doi.org/10.7717/peerj.10792.

744 Huang, Y., B. Wang, X. Li, and H. Wang, 2018: Changes in the influence of the
745 western Pacific subtropical high on Asian summer monsoon rainfall in the late 1990s.
746 *Clim. Dyn.*, **51,** 443-455, http://doi.org/10.1007/s00382-017-3933-1.

747 Huntington, T. G., 2006: Evidence for intensification of the global water cycle:
748 Review and synthesis. *J. Hydrol.*, **319,** 83-95,
749 http://doi.org/https://doi.org/10.1016/j.jhydrol.2005.07.003.

750 Jiang, S., K. Wang, and Y. Mao, 2020: Rapid Local Urbanization around Most
751 Meteorological Stations Explains the Observed Daily Asymmetric Warming Rates
752 across China from 1985 to 2017. *J. Clim.*, **33,** 9045-9061, http://doi.org/10.1175/JCLI-
753 D-20-0118.1.

754 Jong, B.-T., M. Ting, and R. Seager, 2016: El Niño's impact on California
755 precipitation: seasonality, regionality, and El Niño intensity. *Environ. Res. Lett.*, **11,**
756 054021, http://doi.org/10.1088/1748-9326/11/5/054021.

757 Kirchmeier-Young, M. C., and X. Zhang, 2020: Human influence has intensified
758 extreme precipitation in North America. *Proc. Natl. Acad. Sci. U.S.A.*, **117,** 13308,

Accepted for publication in *Journal of Climate*. DOI 10.1175/JCLI-D-21-0324.1.

http://doi.org/10.1073/pnas.1921628117.

Konapala, G., A. K. Mishra, Y. Wada, and M. E. Mann, 2020: Climate change will affect global water availability through compounding changes in seasonal precipitation and evaporation. *Nat. Commun.*, **11,** 3044, http://doi.org/10.1038/s41467-020-16757-w.

Lee, D., S.-K. Min, E. Fischer, H. Shiogama, I. Bethke, L. Lierhammer, and J. F. Scinocca, 2018: Impacts of half a degree additional warming on the Asian summer monsoon rainfall characteristics. *Environ. Res. Lett.*, **13,** 044033, http://doi.org/10.1088/1748-9326/aab55d.

Li, B., Y. Chen, Z. Chen, H. Xiong, and L. Lian, 2016: Why does precipitation in northwest China show a significant increasing trend from 1960 to 2010? *Atmos. Res.*, **167,** 275-284, http://doi.org/https://doi.org/10.1016/j.atmosres.2015.08.017.

Li, W., and Coauthors, 2019: Annual precipitation and daily extreme precipitation distribution: possible trends from 1960 to 2010 in urban areas of China. *Geomatics Nat. Hazards Risk*, **10,** 1694-1711, http://doi.org/10.1080/19475705.2019.1609604.

Li, X., F. Jiang, L. Li, and G. Wang, 2011: Spatial and temporal variability of precipitation concentration index, concentration degree and concentration period in Xinjiang, China. *Int. J. Climatol.*, **31,** 1679-1693, http://doi.org/https://doi.org/10.1002/joc.2181.

Li, Z., S. Yu, L. Wang, K. Mehmood, W. Liu, and K. Alapaty, 2018: Suppression of convective precipitation by elevated man-made aerosols is responsible for large-

780 scale droughts in north China. *Proc. Natl. Acad. Sci. U.S.A.*, **115,** E8327,
781 http://doi.org/10.1073/pnas.1811295115.
782 Liang, L., L. Li, and Q. Liu, 2011: Precipitation variability in Northeast China
783 from 1961 to 2008. *J. Hydrol.*, **404,** 67-76,
784 http://doi.org/https://doi.org/10.1016/j.jhydrol.2011.04.020.
785 Liu, B., M. Xu, M. Henderson, and Y. Qi, 2005: Observed trends of precipitation
786 amount, frequency, and intensity in China, 1960–2000. *J. Geophys. Res.: Atmos.*, **110**,
787 http://doi.org/10.1029/2004JD004864.
788 Liu, Y., Z. Liang, and Y. Li, 2017: Observational and Simulative Study of a Local
789 Severe Precipitation Event Caused by a Cold Vortex over Northeast China. *Adv.*
790 *Meteorol.*, **2017,** 2764340, http://doi.org/10.1155/2017/2764340.
791 Lu, B., and Coauthors, 2019: Impact of El Niño and Southern Oscillation on the
792 summer precipitation over Northwest China. *Atmos. Sci. Lett.*, **20,** e928,
793 http://doi.org/https://doi.org/10.1002/asl.928.
794 Lu, R.-Y., X.-W. Hong, and X.-Y. Li, 2016: Asymmetric association of rainfall and
795 atmospheric circulation over East Asia with anomalous rainfall in the tropical western
796 North Pacific in summer. *Atmos. Oceanic Sci. Lett.*, **9,** 185-190,
797 http://doi.org/10.1080/16742834.2016.1161489.
798 Lv, A., B. Qu, S. Jia, and W. Zhu, 2019: Influence of three phases of El Niño–
799 Southern Oscillation on daily precipitation regimes in China. *Hydrol. Earth Syst. Sci.*,
800 **23,** 883-896, http://doi.org/10.5194/hess-23-883-2019.

Accepted for publication in *Journal of Climate*. DOI 10.1175/JCLI-D-21-0324.1.

Ma, F., A. ye, J. You, and Q. Duan, 2018: 2015–16 floods and droughts in China, and its response to the strong El Niño. *Sci. Total Environ.*, **627,** 1473-1484, http://doi.org/10.1016/j.scitotenv.2018.01.280.

Ma, S., T. Zhou, A. Dai, and Z. Han, 2015: Observed Changes in the Distributions of Daily Precipitation Frequency and Amount over China from 1960 to 2013. *J. Clim.*, **28,** 6960-6978, http://doi.org/10.1175/JCLI-D-15-0011.1.

Ma, S., and Coauthors, 2017: Detectable Anthropogenic Shift toward Heavy Precipitation over Eastern China. *J. Clim.*, **30,** 1381-1396, http://doi.org/10.1175/JCLI-D-16-0311.1.

Mallakpour, I., and G. Villarini, 2017: Analysis of changes in the magnitude, frequency, and seasonality of heavy precipitation over the contiguous USA. *Theor. Appl. Climatol.*, **130,** 1-19, http://doi.org/10.1007/s00704-016-1881-z.

Mann, H. B., 1945: Nonparametric Tests Against Trend. *Econometrica*, **13,** 245-259, http://doi.org/10.2307/1907187.

Mardero, S., B. Schmook, Z. Christman, S. E. Metcalfe, and B. De la Barreda-Bautista, 2020: Recent disruptions in the timing and intensity of precipitation in Calakmul, Mexico. *Theor. Appl. Climatol.*, **140,** 129-144, http://doi.org/10.1007/s00704-019-03068-4.

Miao, C., Q. Duan, Q. Sun, X. Lei, and H. Li, 2019: Non-uniform changes in different categories of precipitation intensity across China and the associated large-scale circulations. *Environ. Res. Lett.*, **14,** 025004, http://doi.org/10.1088/1748-

9326/aaf306.

Myhre, G., and Coauthors, 2019: Frequency of extreme precipitation increases extensively with event rareness under global warming. *Sci. Rep.*, **9,** 16063, http://doi.org/10.1038/s41598-019-52277-4.

Nigam, S., Y. Zhao, A. Ruiz-Barradas, and T. Zhou, 2015a: The South-Flood North-Drought Pattern Over Eastern China and the Drying of the Gangetic Plain. *Climate Change: Multidecadal and Beyond*, WORLD SCIENTIFIC, 347-359.

——, 2015b: The South-Flood North-Drought Pattern Over Eastern China and the Drying of the Gangetic Plain. *Climate Change: Multidecadal and Beyond*, 347-359.

Papalexiou, S. M., and A. Montanari, 2019: Global and Regional Increase of Precipitation Extremes Under Global Warming. *Water Resour. Res.*, **55,** 4901-4914, http://doi.org/https://doi.org/10.1029/2018WR024067.

Pascale, S., V. Lucarini, X. Feng, A. Porporato, and S. u. Hasson, 2015a: Analysis of rainfall seasonality from observations and climate models. *Clim Dyn*, **44,** 3281-3301, http://doi.org/10.1007/s00382-014-2278-2.

——, 2015b: Projected changes of rainfall seasonality and dry spells in a high greenhouse gas emissions scenario. *Clim. Dyn.*, http://doi.org/10.1007/s00382-015-2648-4.

Pendergrass, A. G., and R. Knutti, 2018: The Uneven Nature of Daily Precipitation and Its Change. *Geophys. Res. Lett.*, **45,** 11,980-911,988, http://doi.org/https://doi.org/10.1029/2018GL080298.

Peng, S., and Coauthors, 2013: Precipitation amount, seasonality and frequency regulate carbon cycling of a semi-arid grassland ecosystem in Inner Mongolia, China: A modeling analysis. *Agric. For. Meteorol.*, **178-179,** 46-55, http://doi.org/10.1016/j.agrformet.2013.02.002.

Perkins-Kirkpatrick, S. E., and S. C. Lewis, 2020: Increasing trends in regional heatwaves. *Nat. Commun.*, **11,** 3357, http://doi.org/10.1038/s41467-020-16970-7.

Piao, S., and Coauthors, 2019: Plant phenology and global climate change: Current progresses and challenges. *Global Change Biol.*, **25,** 1922-1940, http://doi.org/10.1111/gcb.14619.

Piao, S., and Coauthors, 2010: The Impacts of Climate Change on Water Resources and Agriculture in China. *Nature*, **467,** 43-51, http://doi.org/10.1038/nature09364.

Pryor, S. C., and J. T. Schoof, 2008: Changes in the seasonality of precipitation over the contiguous USA. *J. Geophys. Res.: Atmos.*, **113**, http://doi.org/https://doi.org/10.1029/2008JD010251.

Qian, W., and X. Lin, 2005: Regional trends in recent precipitation indices in China. *Meteorol. Atmos. Phys.*, **90,** 193-207, http://doi.org/10.1007/s00703-004-0101-z.

Rohr, T., S. Manzoni, X. Feng, R. S. C. Menezes, and A. Porporato, 2013: Effect of rainfall seasonality on carbon storage in tropical dry ecosystems. *J. Geophys. Res.: Biogeosci.*, **118,** 1156-1167, http://doi.org/10.1002/jgrg.20091.

Accepted for publication in *Journal of Climate*. DOI 10.1175/JCLI-D-21-0324.1.

Sahany, S., S. K. Mishra, R. Pathak, and B. Rajagopalan, 2018: Spatiotemporal Variability of Seasonality of Rainfall Over India. *Geophys. Res. Lett.*, **45,** 7140-7147, http://doi.org/10.1029/2018GL077932.

Sen, P. K., 1968: Estimates of the Regression Coefficient Based on Kendall's Tau. *J. Am. Stat. Assoc.*, **63,** 1379-1389, http://doi.org/10.1080/01621459.1968.10480934.

Sha, Y., Z. Shi, X. Liu, Z. An, X. Li, and H. Chang, 2018: Role of the Tian Shan Mountains and Pamir Plateau in Increasing Spatiotemporal Differentiation of Precipitation over Interior Asia. *J. Clim.*, **31,** 8141-8162, http://doi.org/10.1175/JCLI-D-17-0594.1.

Shi, P., and Coauthors, 2014: Climate change regionalization in China (196Q 2010). *Science China Earth Sciences*, **57,** 2676-2689,

Shi, Y., Y. Shen, E. Kang, D. Li, Y. Ding, G. Zhang, and R. Hu, 2007: Recent and Future Climate Change in Northwest China. *Clim. Change*, **80,** 379-393, http://doi.org/10.1007/s10584-006-9121-7.

Shin, J., and S. Park, 2020: Impacts of ENSO and Madden–Julian oscillation on the genesis of tropical cyclones simulated by general circulation models and compared to observations. *Environ. Res. Lett.*, **15,** 034046, http://doi.org/10.1088/1748-9326/ab7466.

Song, F., L. R. Leung, J. Lu, and L. Dong, 2018: Seasonally dependent responses of subtropical highs and tropical rainfall to anthropogenic warming. *Nat. Clim. Change*, **8,** 787-792, http://doi.org/10.1038/s41558-018-0244-4.

Accepted for publication in *Journal of Climate*. DOI 10.1175/JCLI-D-21-0324.1.

885 Song, F., J. Lu, L. R. Leung, and F. Liu, 2020: Contrasting Phase Changes of
886 Precipitation Annual Cycle Between Land and Ocean Under Global Warming. *Geophys.*
887 *Res. Lett.*, **47,** e2020GL090327, http://doi.org/https://doi.org/10.1029/2020GL090327.
888 Song, F., L. R. Leung, J. Lu, L. Dong, W. Zhou, B. Harrop, and Y. Qian, 2021:
889 Emergence of seasonal delay of tropical rainfall during 1979–2019. *Nat. Clim. Change*,
890 http://doi.org/10.1038/s41558-021-01066-x.
891 Sun, J., and F. Zhang, 2017: Daily extreme precipitation and trends over China.
892 *Science China Earth Sciences*, **60**, http://doi.org/10.1007/s11430-016-9117-8.
893 Sun, Q., C. Miao, and Q. Duan, 2017: Changes in the Spatial Heterogeneity and
894 Annual Distribution of Observed Precipitation across China. *J. Clim.*, **30,** 9399-9416,
895 http://doi.org/10.1175/JCLI-D-17-0045.1.
896 Sun, Q., C. Miao, A. AghaKouchak, I. Mallakpour, D. Ji, and Q. Duan, 2020:
897 Possible Increased Frequency of ENSO-Related Dry and Wet Conditions over Some
898 Major Watersheds in a Warming Climate. *Bull. Am. Meteorol. Soc.*, **101,** E409-E426,
899 http://doi.org/10.1175/BAMS-D-18-0258.1.
900 Tan, X., Y. Wu, B. Liu, and S. Chen, 2020: Inconsistent changes in global
901 precipitation seasonality in seven precipitation datasets. *Clim. Dyn.*, **54**,
902 http://doi.org/10.1007/s00382-020-05158-w.
903 Tao, Y., W. Wang, S. Song, and J. Ma, 2018: Spatial and Temporal Variations of
904 Precipitation Extremes and Seasonality over China from 1961~2013. *Water*, **10,** 719,
905 http://doi.org/10.3390/w10060719.

Accepted for publication in *Journal of Climate*. DOI 10.1175/JCLI-D-21-0324.1.

906 Teegavarapu, R. S. V., A. Goly, and J. Obeysekera, 2013: Influences of Atlantic
907 multidecadal oscillation phases on spatial and temporal variability of regional
908 precipitation extremes. *J. Hydrol.*, **495,** 74-93,
909 http://doi.org/https://doi.org/10.1016/j.jhydrol.2013.05.003.
910 Tian, F., B. Dong, J. Robson, and R. Sutton, 2018: Forced decadal changes in the
911 East Asian summer monsoon: the roles of greenhouse gases and anthropogenic aerosols.
912 *Clim. Dyn.*, **51,** 3699-3715, http://doi.org/10.1007/s00382-018-4105-7.
913 Tian, Q., M. Prange, and U. Merkel, 2016: Precipitation and temperature changes
914 in the major Chinese river basins during 1957-2013 and links to sea surface temperature.
915 *J. Hydrol.*, **536**, http://doi.org/10.1016/j.jhydrol.2016.02.048.
916 Trenberth, K. E., 2011: Changes in precipitation with climate change. *Climate*
917 *Research*, **47,** 123-138,
918 Villarreal, S., and Coauthors, 2016: Contrasting precipitation seasonality
919 influences evapotranspiration dynamics in water-limited shrublands. *J. Geophys. Res.:*
920 *Biogeosci.*, **121,** 494-508, http://doi.org/10.1002/2015JG003169.
921 Wang, J., Y. Chen, S. F. B. Tett, Z. Yan, P. Zhai, J. Feng, and J. Xia, 2020a:
922 Anthropogenically-driven increases in the risks of summertime compound hot extremes.
923 *Nat. Commun.*, **11,** 528, http://doi.org/10.1038/s41467-019-14233-8.
924 Wang, Q., P.-M. Zhai, and D.-H. Qin, 2020b: New perspectives on 'warming–
925 wetting' trend in Xinjiang, China. *Adv. Clim. Change Res.*, **11,** 252-260,
926 http://doi.org/https://doi.org/10.1016/j.accre.2020.09.004.

Accepted for publication in *Journal of Climate*. DOI 10.1175/JCLI-D-21-0324.1.

927 Wang, S. Y. S., J.-H. Yoon, E. Becker, and R. Gillies, 2017a: California from
928 drought to deluge. *Nat. Clim. Change*, **7,** 465-468, http://doi.org/10.1038/nclimate3330.
929 Wang, T.-J., J.-Z. Min, Y.-F. Xu, and K.-S. Lam, 2003: Seasonal variations of
930 anthropogenic sulfate aerosol and direct radiative forcing over China. *Meteorol. Atmos.*
931 *Phys.*, **84,** 185-198, http://doi.org/10.1007/s00703-002-0581-7.
932 Wang, Y., B. Zhou, D. Qin, J. Wu, R. Gao, and L. Song, 2017b: Changes in mean
933 and extreme temperature and precipitation over the arid region of northwestern China:
934 Observation and projection. *Adv. Atmos. Sci.*, **34,** 289-305,
935 http://doi.org/10.1007/s00376-016-6160-5.
936 Ward, P. J., B. Jongman, M. Kummu, M. D. Dettinger, F. C. Sperna Weiland, and
937 H. C. Winsemius, 2014: Strong influence of El Niño Southern Oscillation on flood risk
938 around the world. *Proc. Natl. Acad. Sci. U.S.A.*, **111,** 15659-15664,
939 http://doi.org/10.1073/pnas.1409822111.
940 Welhouse, L. J., M. A. Lazzara, L. M. Keller, G. J. Tripoli, and M. H. Hitchman,
941 2016: Composite Analysis of the Effects of ENSO Events on Antarctica. *J. Clim.*, **29,**
942 1797-1808, http://doi.org/10.1175/JCLI-D-15-0108.1.
943 Wu, G., and Coauthors, 2016: Advances in studying interactions between aerosols
944 and monsoon in China. *Science China Earth Sciences*, **59,** 1-16,
945 http://doi.org/10.1007/s11430-015-5198-z.
946 Wu, P., Y. Ding, Y. Liu, and X. Li, 2019: The characteristics of moisture recycling
947 and its impact on regional precipitation against the background of climate warming over

Accepted for publication in *Journal of Climate*. DOI 10.1175/JCLI-D-21-0324.1.

948 Northwest China. *Int. J. Climatol.*, **39,** 5241-5255,
949 http://doi.org/https://doi.org/10.1002/joc.6136.

950 Xie, Z., A. Duan, and Q. Tian, 2017: Weighted composite analysis and its
951 application: an example using ENSO and geopotential height. *Atmos. Sci. Lett.*, **18,** 435-
952 440, http://doi.org/https://doi.org/10.1002/asl.786.

953 Xu, W., C. Sun, J. Zuo, Z. Ma, W. Li, and S. Yang, 2019: Homogenization of
954 Monthly Ground Surface Temperature in China during 1961–2016 and Performances
955 of GLDAS Reanalysis Products. *J. Clim.*, **32,** 1121-1135, http://doi.org/10.1175/JCLI-
956 D-18-0275.1.

957 Xue, F., P. Amilcare, and R.-I. Ignacio, 2013: Changes in rainfall seasonality in
958 the tropics. *Nat. Clim. Change*, **3,** 811, http://doi.org/10.1038/nclimate1907.

959 Yan, D., X. Zhang, Y. Yu, W. Guo, and N. P. Hanan, 2016: Characterizing land
960 surface phenology and responses to rainfall in the Sahara desert. *J. Geophys. Res.:*
961 *Biogeosci.*, **121,** 2243-2260, http://doi.org/10.1002/2016JG003441.

962 Yang Jianping, D. Y., Chen Rensheng, Liu Lianyou, 2002: The Interdecadal
963 Fluctuation of Dry and Wet Climate Boundaries in China in Recent 50 Years. *Acta*
964 *Geographica Sinica*, **57,** 655-661, http://doi.org/10.11821/xb200206004.

965 Yao, J., Y. Chen, Y. Zhao, W. Mao, X. Xu, Y. Liu, and Q. Yang, 2018: Response
966 of vegetation NDVI to climatic extremes in the arid region of Central Asia: a case study
967 in Xinjiang, China. *Theor. Appl. Climatol.*, **131,** 1503-1515,
968 http://doi.org/10.1007/s00704-017-2058-0.

Accepted for publication in *Journal of Climate*. DOI 10.1175/JCLI-D-21-0324.1.

969 Yu, S., and Coauthors, 2016: Anthropogenic aerosols are a potential cause for
970 migration of the summer monsoon rain belt in China. *Proc. Natl. Acad. Sci. U.S.A.*, **113,**
971 E2209, http://doi.org/10.1073/pnas.1601104113.
972 Yun, J., S.-J. Jeong, C.-H. Ho, C.-E. Park, H. Park, and J. Kim, 2018: Influence of
973 winter precipitation on spring phenology in boreal forests. *Global Change Biol.*, **24,**
974 5176-5187, http://doi.org/10.1111/gcb.14414.
975 Zeppel, M. J. B., J. V. Wilks, and J. D. Lewis, 2014: Impacts of extreme
976 precipitation and seasonal changes in precipitation on plants. *Biogeosciences*, **11,** 3083-
977 3093, http://doi.org/10.5194/bg-11-3083-2014.
978 Zhai, P., X. Zhang, H. Wan, and X. Pan, 2005: Trends in Total Precipitation and
979 Frequency of Daily Precipitation Extremes over China. *J. Clim.*, **18,** 1096-1108,
980 Zhang, J., and Coauthors, 2018: Effects of seasonal variability of climatic factors
981 on vegetation coverage across drylands in northern China. *Land Degrad. Dev.*, **29,**
982 1782-1791, http://doi.org/10.1002/ldr.2985.
983 Zhang, Q., J. Lin, W. Liu, and L. Han, 2019a: Precipitation seesaw phenomenon
984 and its formation mechanism in the eastern and western parts of Northwest China
985 during the flood season. *Science China Earth Sciences*, **62**,
986 Zhang, R., A. Sumi, and M. Kimoto, 1999: A diagnostic study of the impact of El
987 Niño on the precipitation in China. *Adv. Atmos. Sci.*, **16,** 229-241,
988 http://doi.org/10.1007/BF02973084.
989 Zhang, R., Q. Min, and J. Su, 2017: Impact of El Niño on atmospheric circulations

Accepted for publication in *Journal of Climate*. DOI 10.1175/JCLI-D-21-0324.1.

over East Asia and rainfall in China: Role of the anomalous western North Pacific anticyclone. *Science China Earth Sciences*, **60,** 1124-1132, http://doi.org/10.1007/s11430-016-9026-x.

Zhang, W., T. Zhou, L. Zhang, and L. Zou, 2019b: Future Intensification of the Water Cycle with an Enhanced Annual Cycle over Global Land Monsoon Regions. *J. Clim.*, **32,** 5437-5452, http://doi.org/10.1175/JCLI-D-18-0628.1.

Zhang, Y., M. P. Dannenberg, T. Hwang, and C. Song, 2019c: El Niño-Southern Oscillation-Induced Variability of Terrestrial Gross Primary Production During the Satellite Era. *J. Geophys. Res.: Biogeosci.*, **124,** 2419-2431, http://doi.org/10.1029/2019JG005117.

Zheng, J., J. Bian, Q. Ge, Z. Hao, Y. Yin, and Y. Liao, 2013: The climate regionalization in China for 1981-2010. *Chin. Sci. Bull.*, **58,** 3088, http://doi.org/https://doi.org/10.1360/972012-1491.

Zhou, B., Y. Xu, J. Wu, S. Dong, and Y. Shi, 2016: Changes in temperature and precipitation extreme indices over China: analysis of a high-resolution grid dataset. *Int. J. Climatol.*, **36,** 1051-1066, http://doi.org/https://doi.org/10.1002/joc.4400.

Accepted for publication in *Journal of Climate*. DOI 10.1175/JCLI-D-21-0324.1.

1009 **FIGURES**

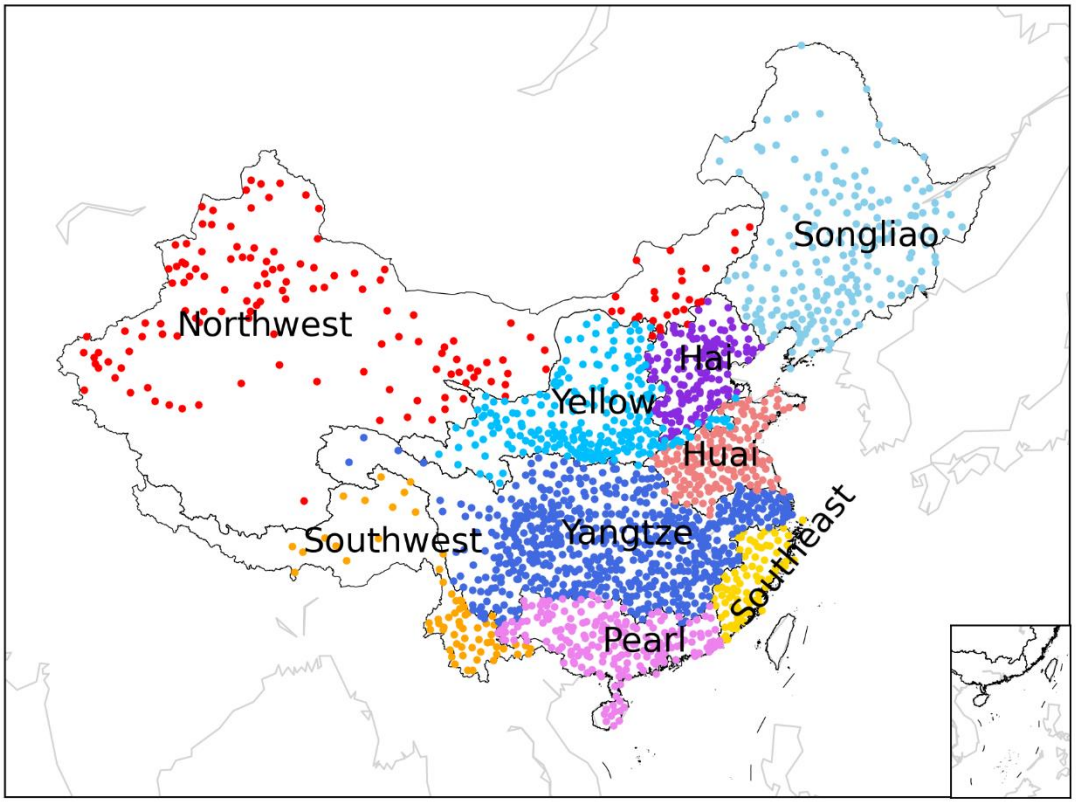

1010

1011 Figure 1 Rain gauge stations in China nine river basins: Northwest River basin, Hai

1012 River basin, Songliao River basin, Yellow River basin, Huai River basin, Southwest

1013 River basin, Yangtze River basin, Pearl River basin, and Southeast River basin.

1014

1015

1016

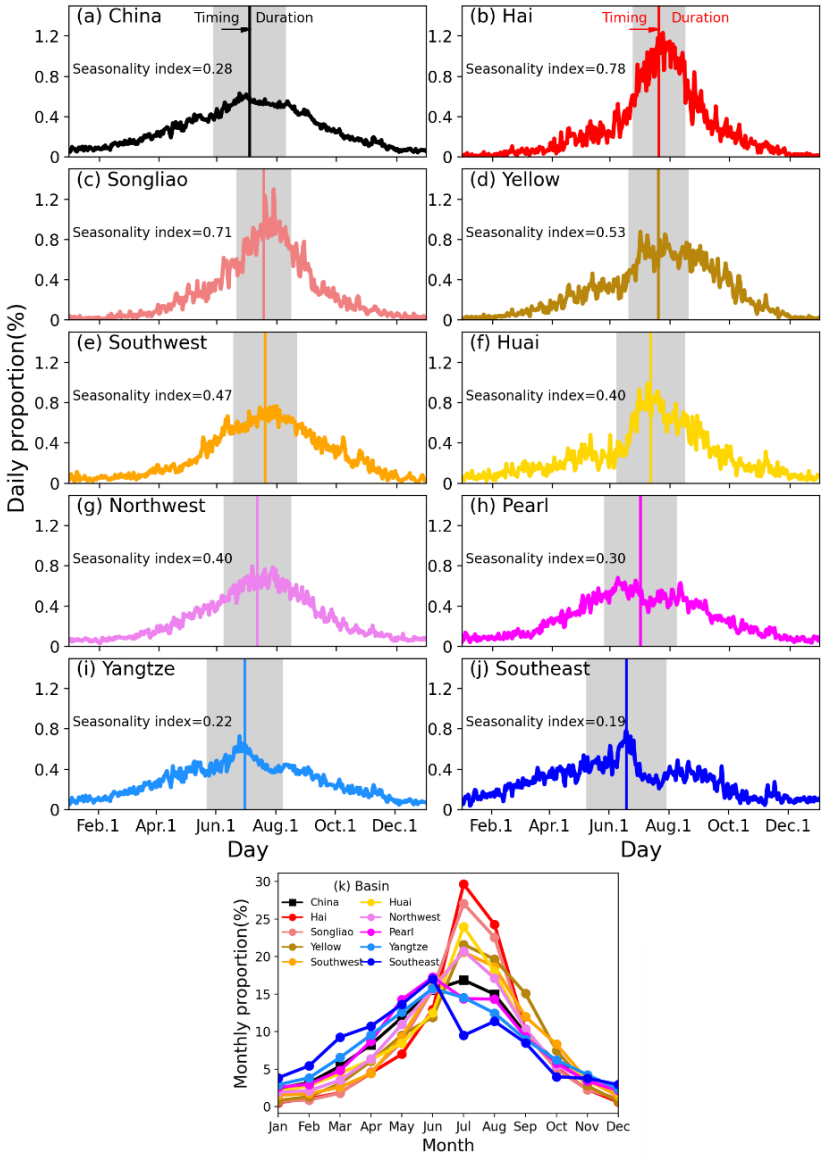

1017

1018 Figure 2 Multiyear mean daily and monthly precipitation proportion accounting for

1019 the annual mean precipitation in China and its nine major basins from 1960 to 2018.

1020 The nine river basins are (a) Hai River basin, (b) Songliao River basin, (c) Yellow

1021 River basin, (d) Southwest River basin, (e) Huai River basin, (f) Northwest River

1022 basin, (j) Pearl River basin, (h) Yangtze River basin, (i) Southeast River basin. (k)

1023 indicates the monthly precipitation proportion. The shaded area from (a)~(j) is the

1024 duration of wet season with the central line indicating the timing of wet season.

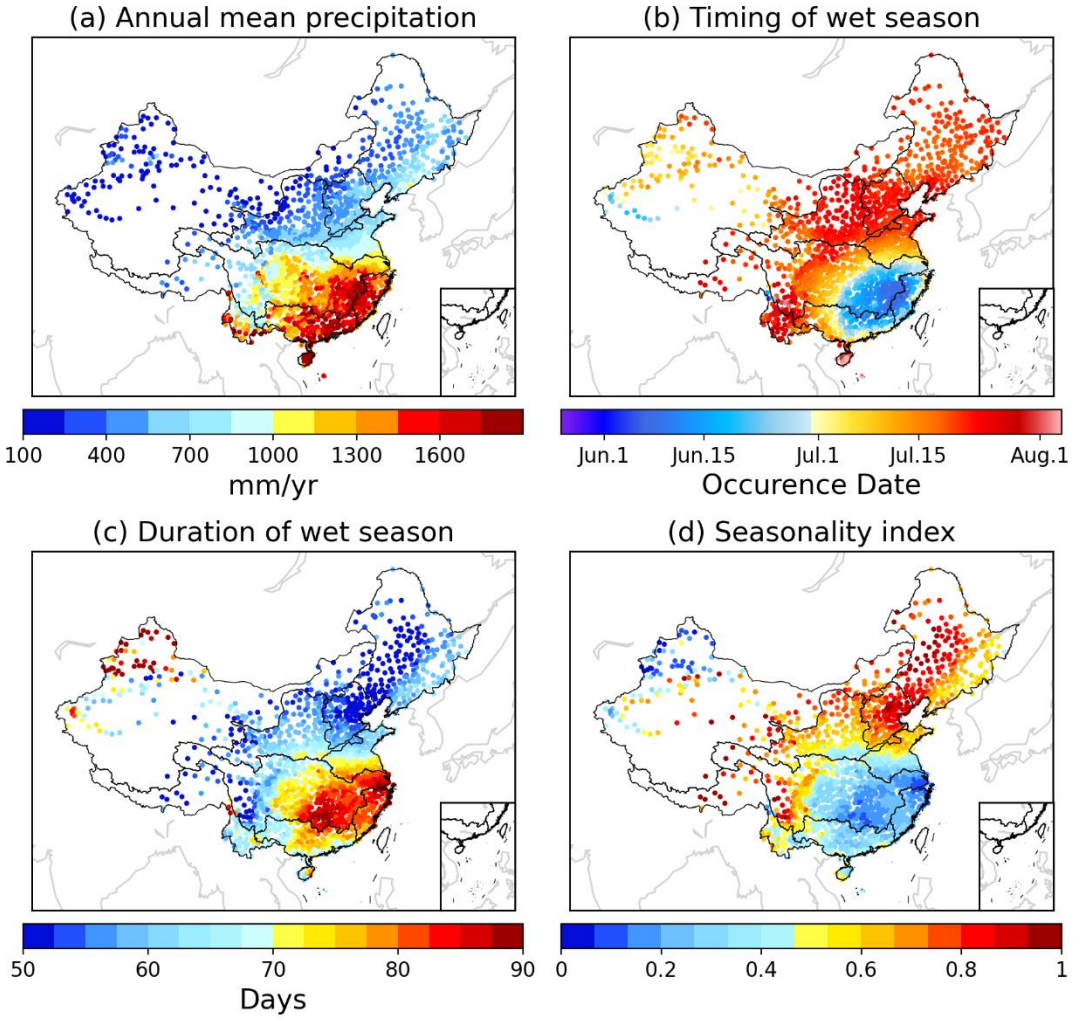

1025

1026 Figure 3 Multiyear mean precipitation seasonality components at China gauge stations

1027 from 1960 to 2018. (a) Annual mean precipitation. (b) Timing of the wet season. (c)

1028 Duration of the wet season. (d) Seasonality index.

1029

Accepted for publication in *Journal of Climate*. DOI 10.1175/JCLI-D-21-0324.1.

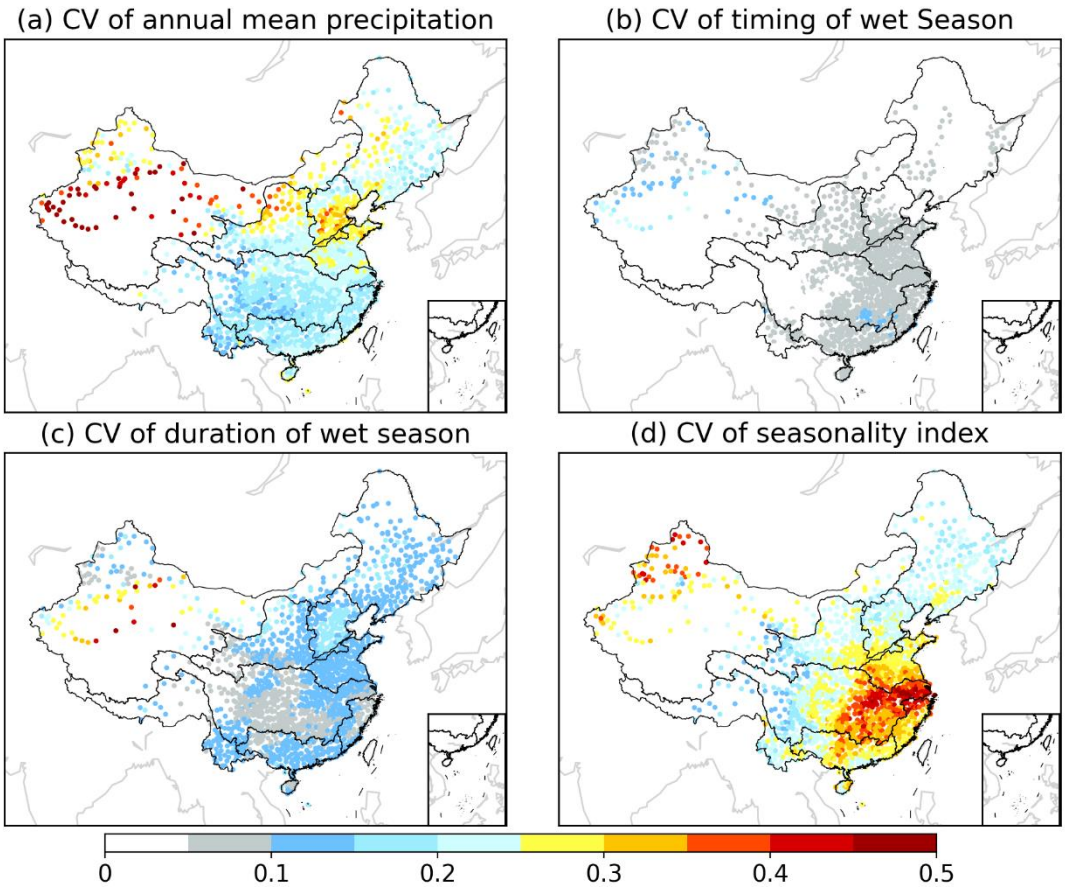

Figure 4 Coefficient of variation (CV) of annual mean precipitation (a), timing of the wet season (b), duration of wet season (c) and seasonality index (d) during the period of 1960-2018.

Accepted for publication in *Journal of Climate*. DOI 10.1175/JCLI-D-21-0324.1.

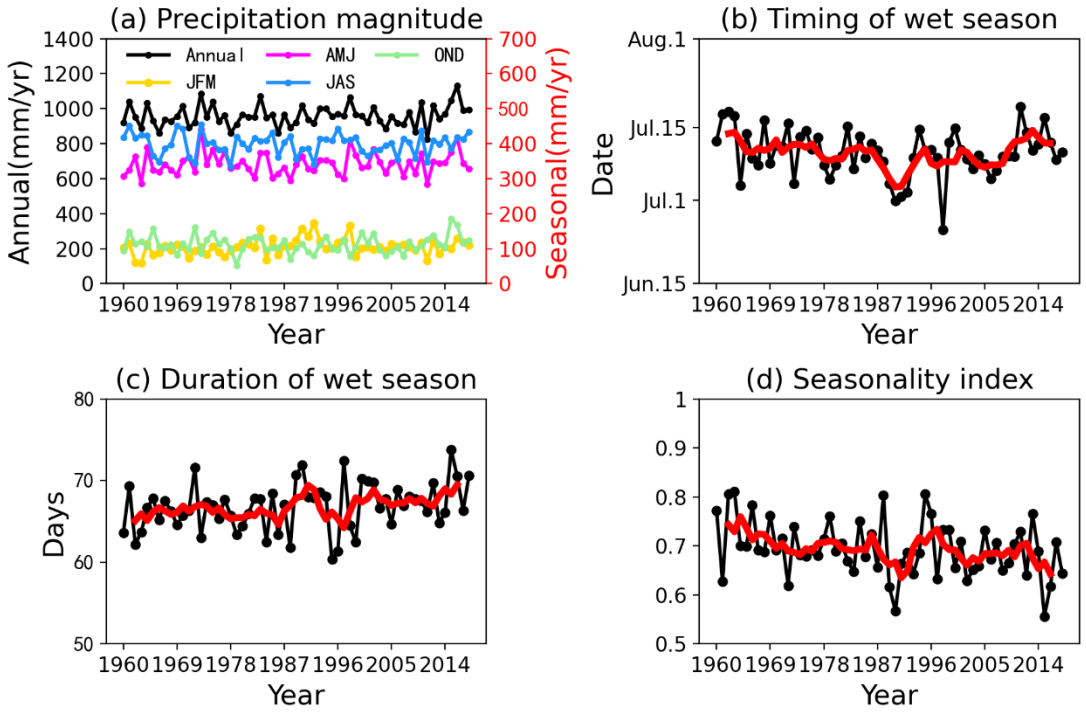

Figure 5 Annual time series of precipitation seasonality indices in China. (a) Annual and seasonal magnitudes (January–March (JFM), April-June (AMJ) and July–September (JAS), October–December (OND)). The left axis is for annual precipitation, and the right axis is for seasonal precipitation. (b) Timing of the wet season, (c) Duration of the wet season and (d) Seasonality index. The 5-year moving average of each variable is shown by the thick red lines.

Accepted for publication in *Journal of Climate*. DOI 10.1175/JCLI-D-21-0324.1.

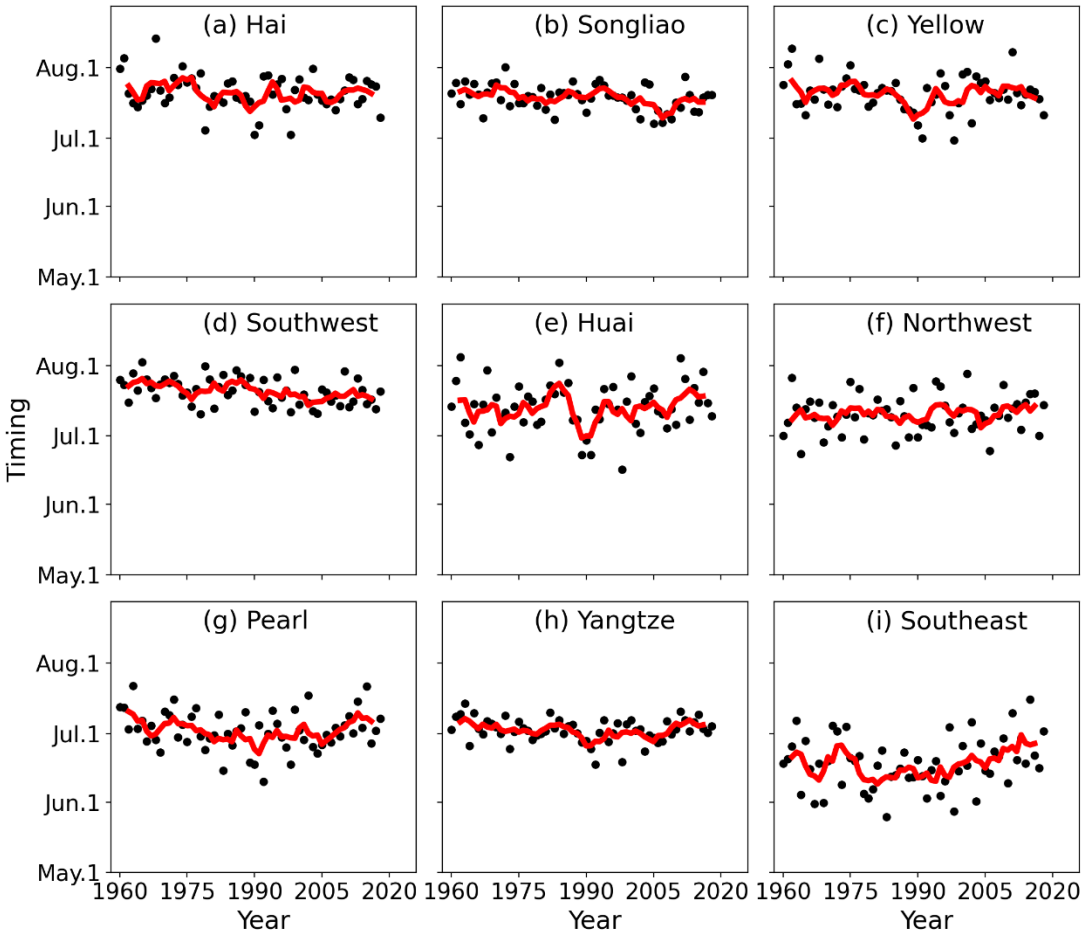

1048

1049 Figure 6 Annual timing of wet season from 1960 to 2018 in China nine river basins i.e.,

1050 Northwest River basin, Hai River basin, Songliao River basin, Yellow River basin, Huai

1051 River basin, Southwest River basin, Yangtze River basin, Pearl River basin, and

1052 Southeast River basin. The 5-year moving average of each variable is shown in red

1053 thick lines.

1054

Accepted for publication in *Journal of Climate*. DOI 10.1175/JCLI-D-21-0324.1.

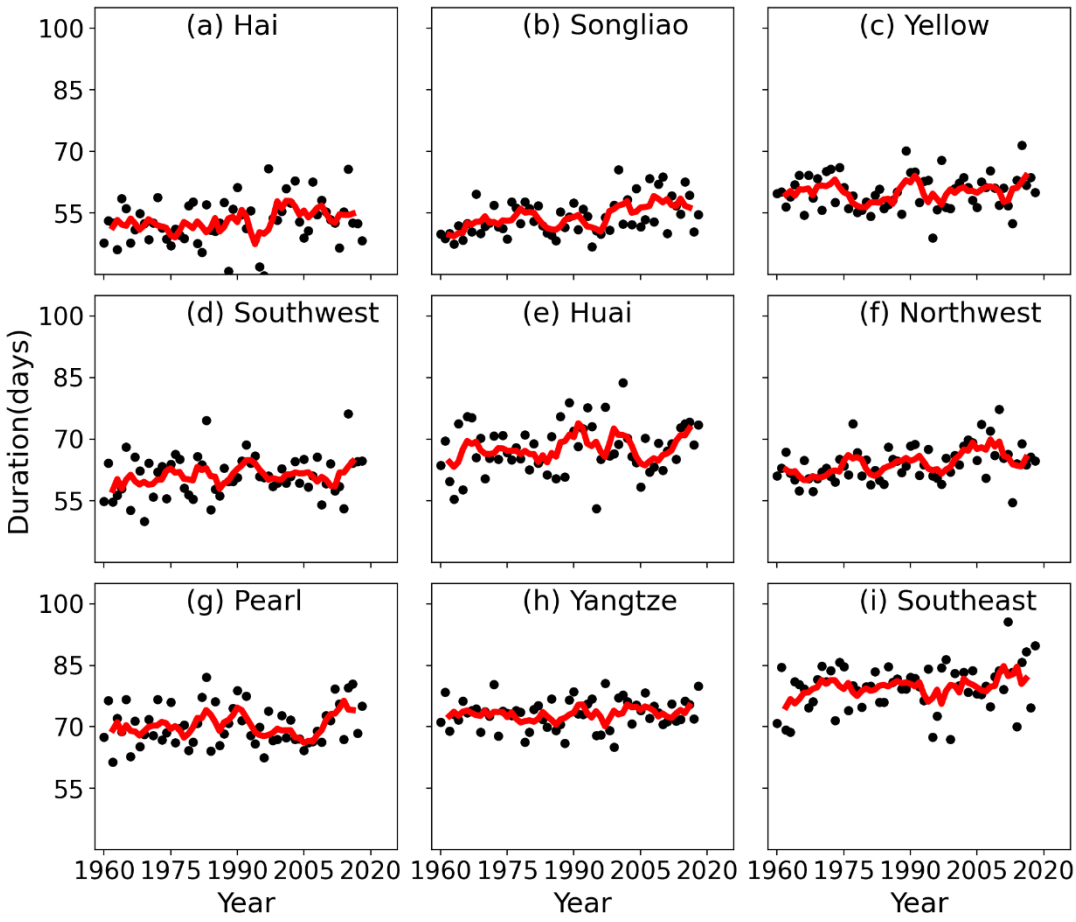

Figure 7 Annual duration of wet season from 1960 to 2018 in China nine river basins i.e., Northwest River basin, Hai River basin, Songliao River basin, Yellow River basin, Huai River basin, Southwest River basin, Yangtze River basin, Pearl River basin, and Southeast River basin. The 5-year moving average of each variable is shown in red thick lines.

Accepted for publication in *Journal of Climate*. DOI 10.1175/JCLI-D-21-0324.1.

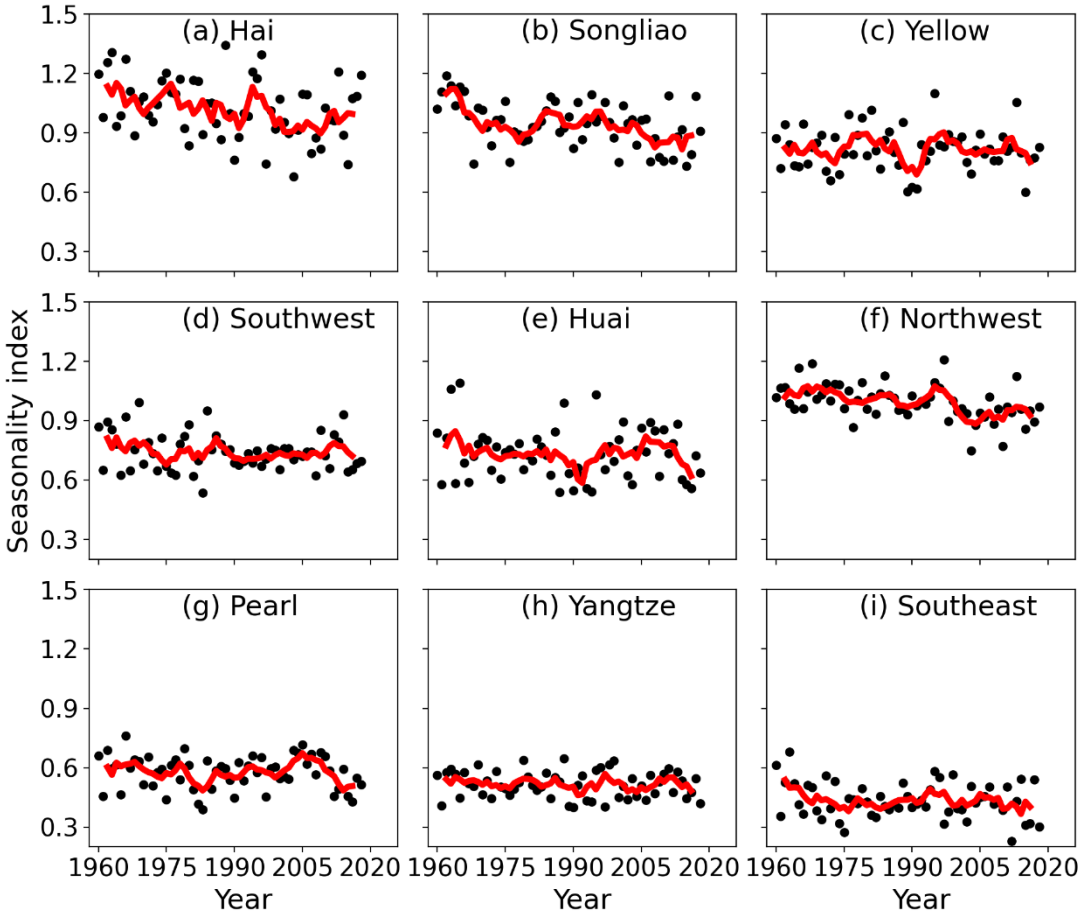

Figure 8 Annual seasonality index from 1960 to 2018 in China nine river basins i.e., Northwest River basin, Hai River basin, Songliao River basin, Yellow River basin, Huai River basin, Southwest River basin, Yangtze River basin, Pearl River basin, and Southeast River basin. The 5-year moving average of each variable is shown in red thick lines.

Accepted for publication in *Journal of Climate*. DOI 10.1175/JCLI-D-21-0324.1.

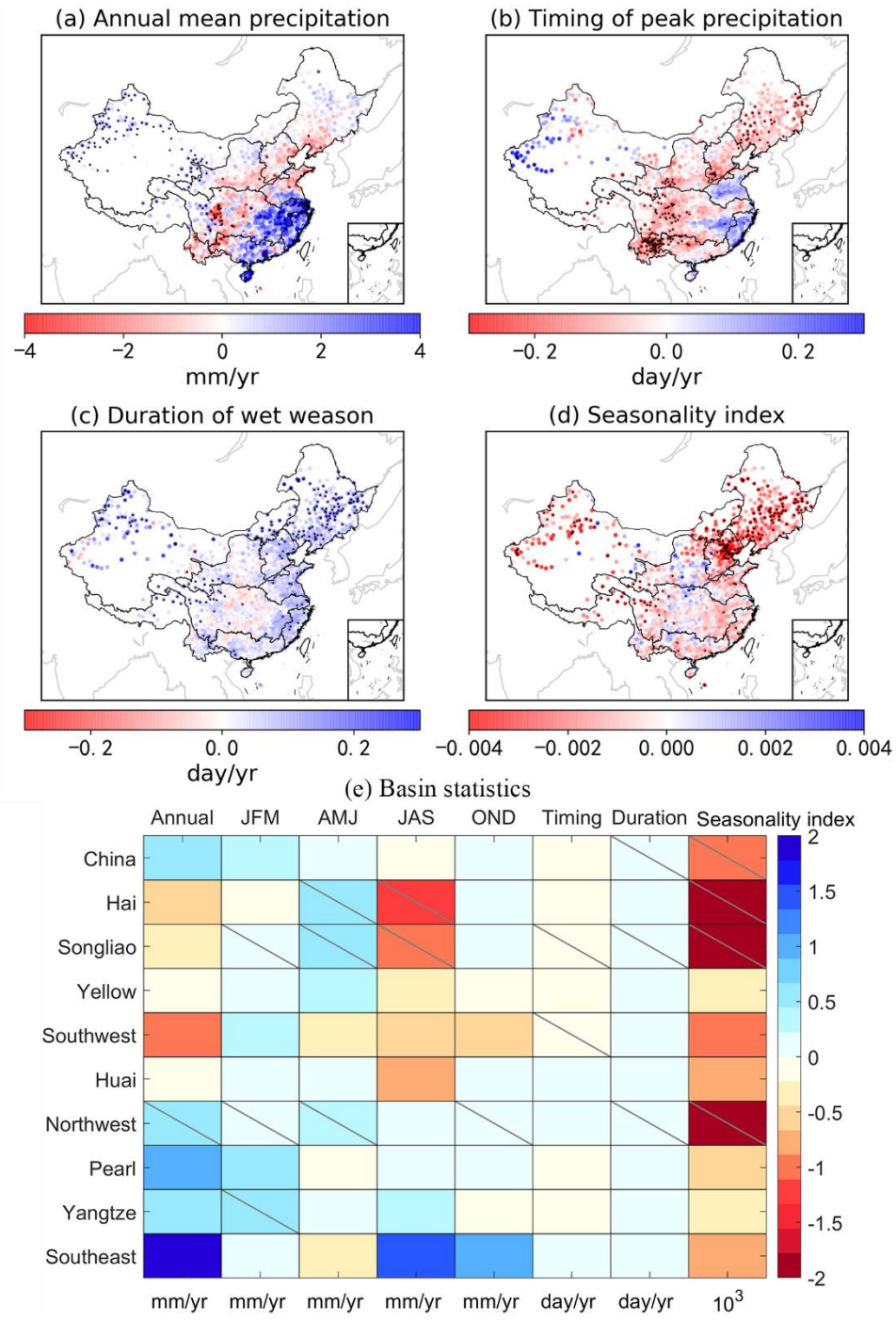

1071

1072 Figure 9 Long-term trends of precipitation seasonality components from 1960 to 2018

1073 at station (a, b, c, d) and basin scale (e). Black dots in (a, b, c, d) and the hatch in the

1074 box in (e) indicate significant changes at the p=0.05 level. In (e), each column indicates

1075 one seasonality indicator and each line indicates one river basin. The units of each

1076 indicator are shown at bottom.

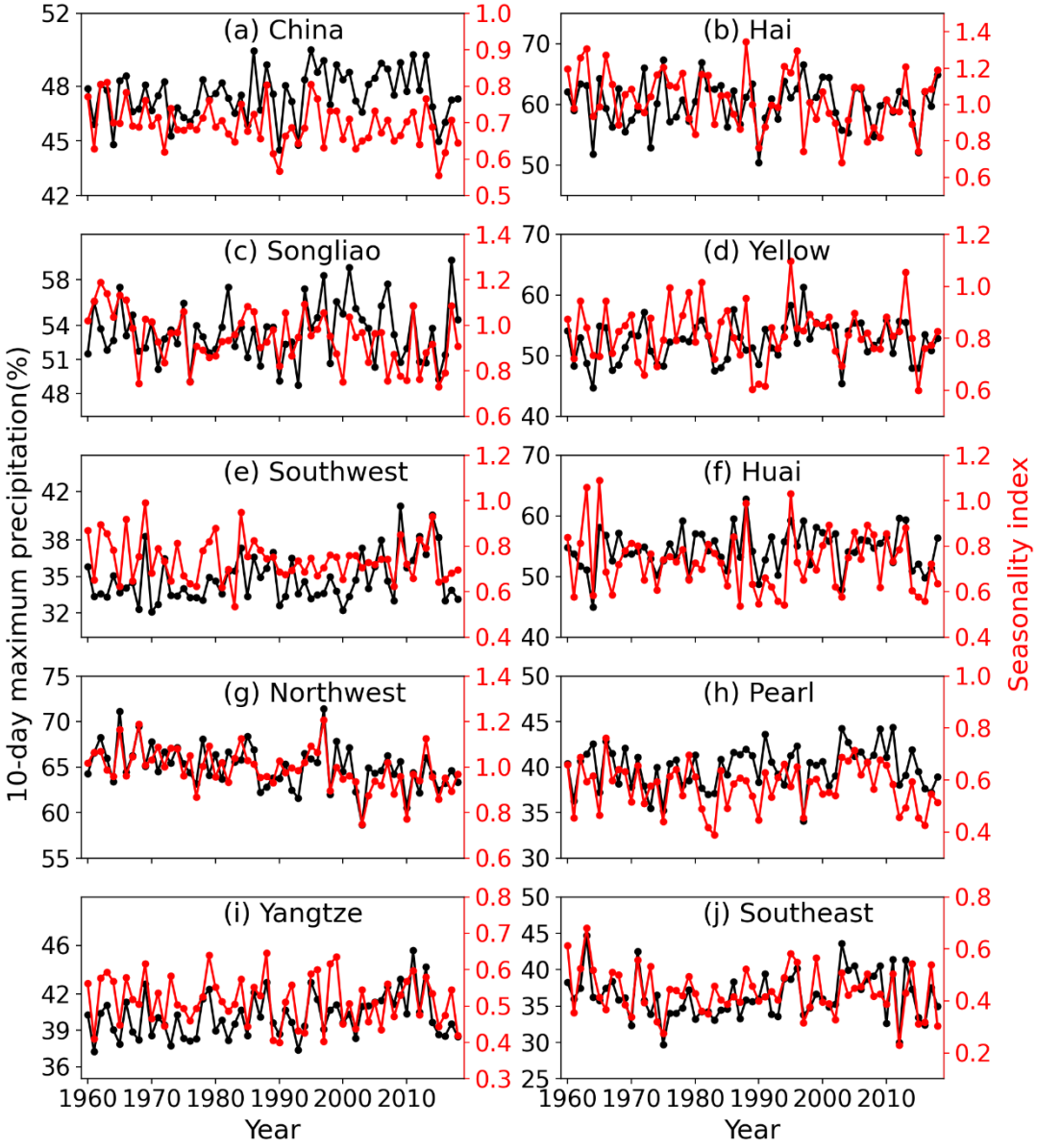

Figure 10 Time series of annual proportion of 10-day maximum precipitation in annual precipitation (black line) and annual seasonality index (red line) from 1960 to 2018 in China (a) and nine of its river basins, i.e., (b) Hai River basin, (c) Songliao River basin, (d) Yellow River basin, (e) Southwest River basin, (f) Huai River basin, (g) Northwest River basin, (h) Pearl River basin, (i) Yangtze River basin and (j) Southeast River basin. The annual proportion is shown on the left axis, and the annual seasonality index is shown on the right axis.

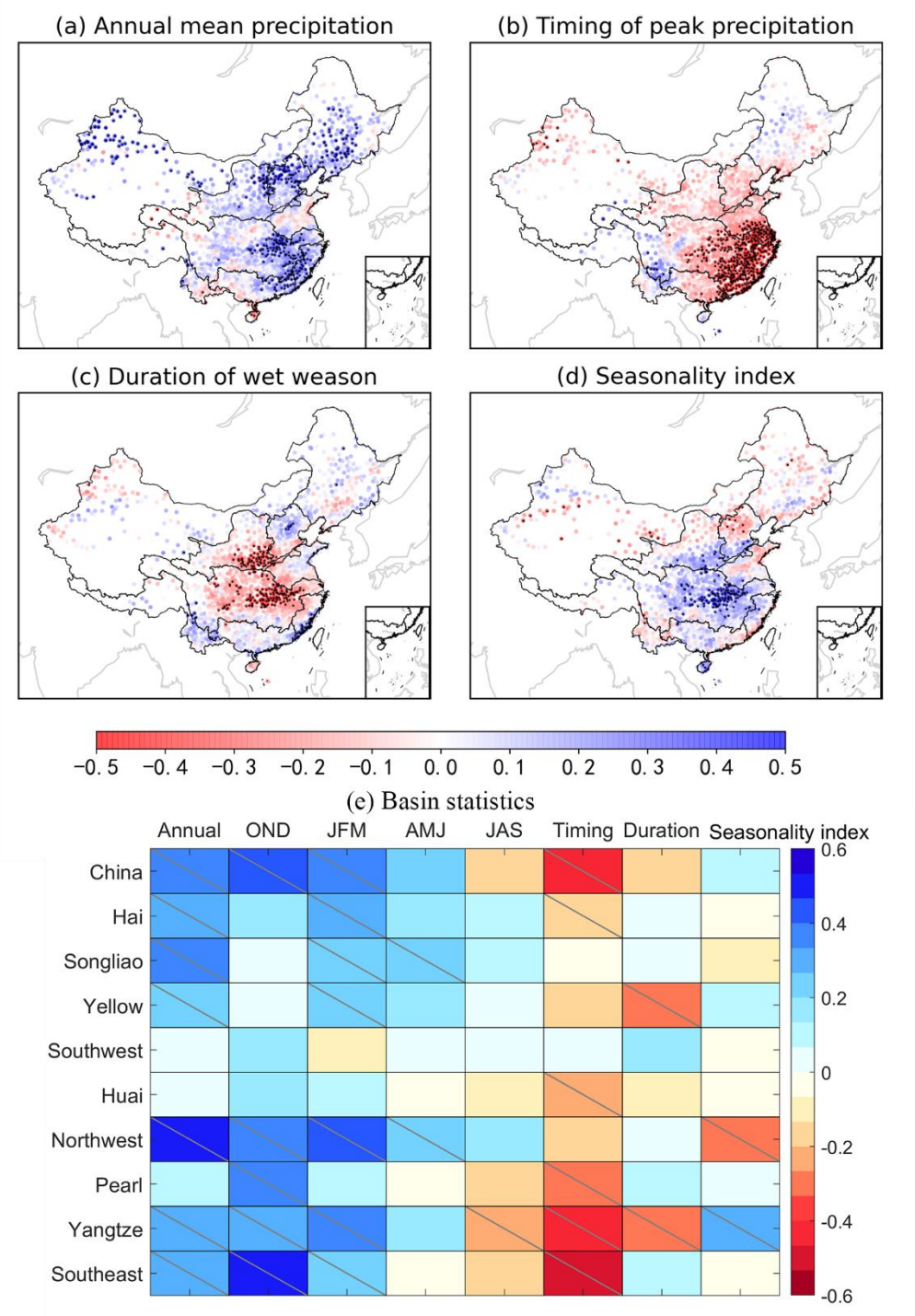

1085

1086 Figure 11 Correlation coefficient of precipitation seasonality indices and Niño-3.4

1087 index at station (a, b, c, d) and basin scale (e). Black dots in (a, b, c, d) indicate a

1088 significant change at the p=0.05 level and the hatch in the box in (e) indicates

1089 significant changes at the p=0.05 level.

Accepted for publication in *Journal of Climate*. DOI 10.1175/JCLI-D-21-0324.1.

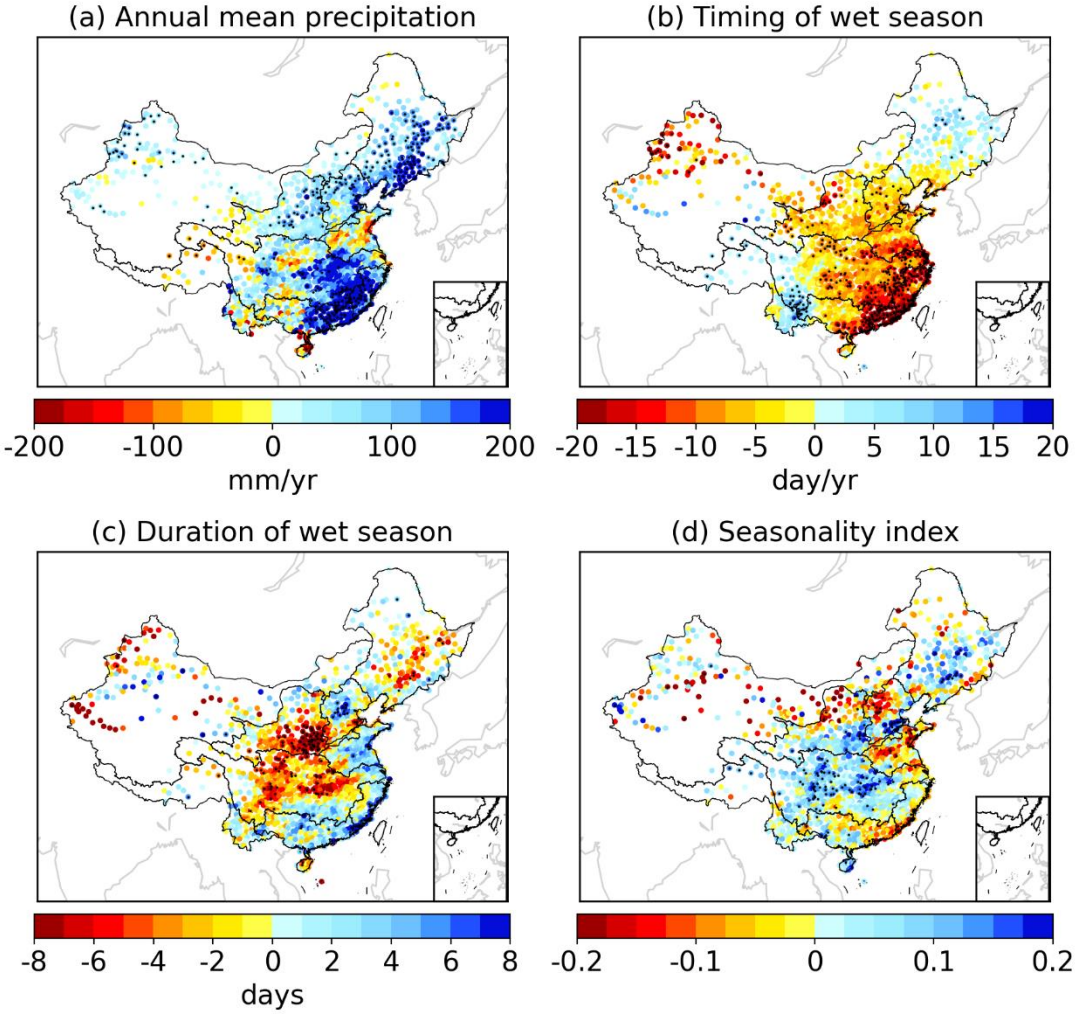

1090

1091 Figure 12 Composite differences in precipitation seasonality indices between strong EI

1092 Niño years and La Niña years during the period of 1960 and 2018. Black dots indicate

1093 a significant change at the p=0.05 level.

1094

Accepted for publication in *Journal of Climate*. DOI 10.1175/JCLI-D-21-0324.1.

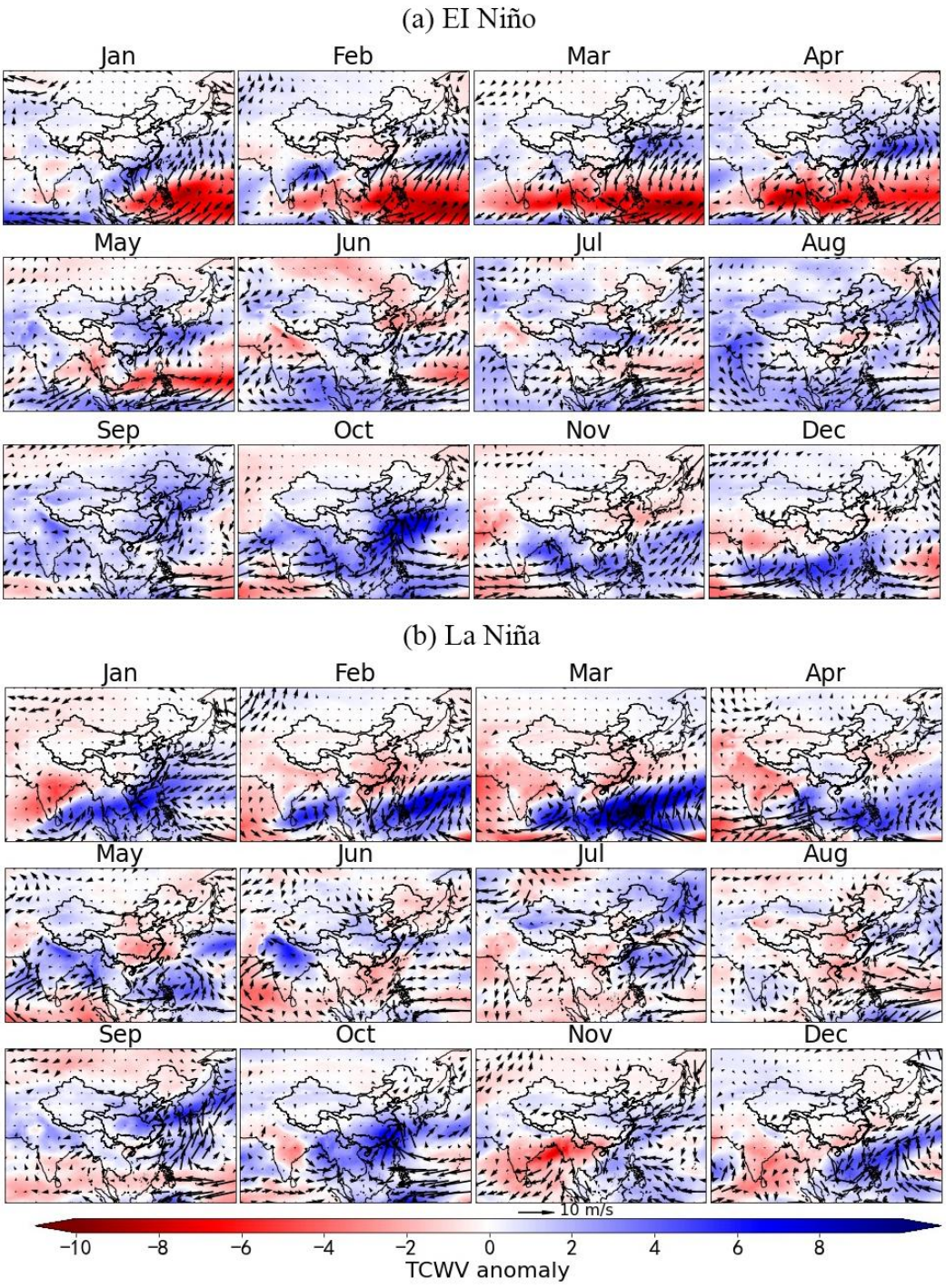

Figure 13 Monthly anomaly of the total column water vapor (TCWV) (shading, unit: $kg \cdot m^{-2} \cdot s^{-1}$) in strong EI Niño and strong La Niña years from 1960 to 2018. The vector arrows indicate wind anomalies, and the direction indicates the direction of wind speed.

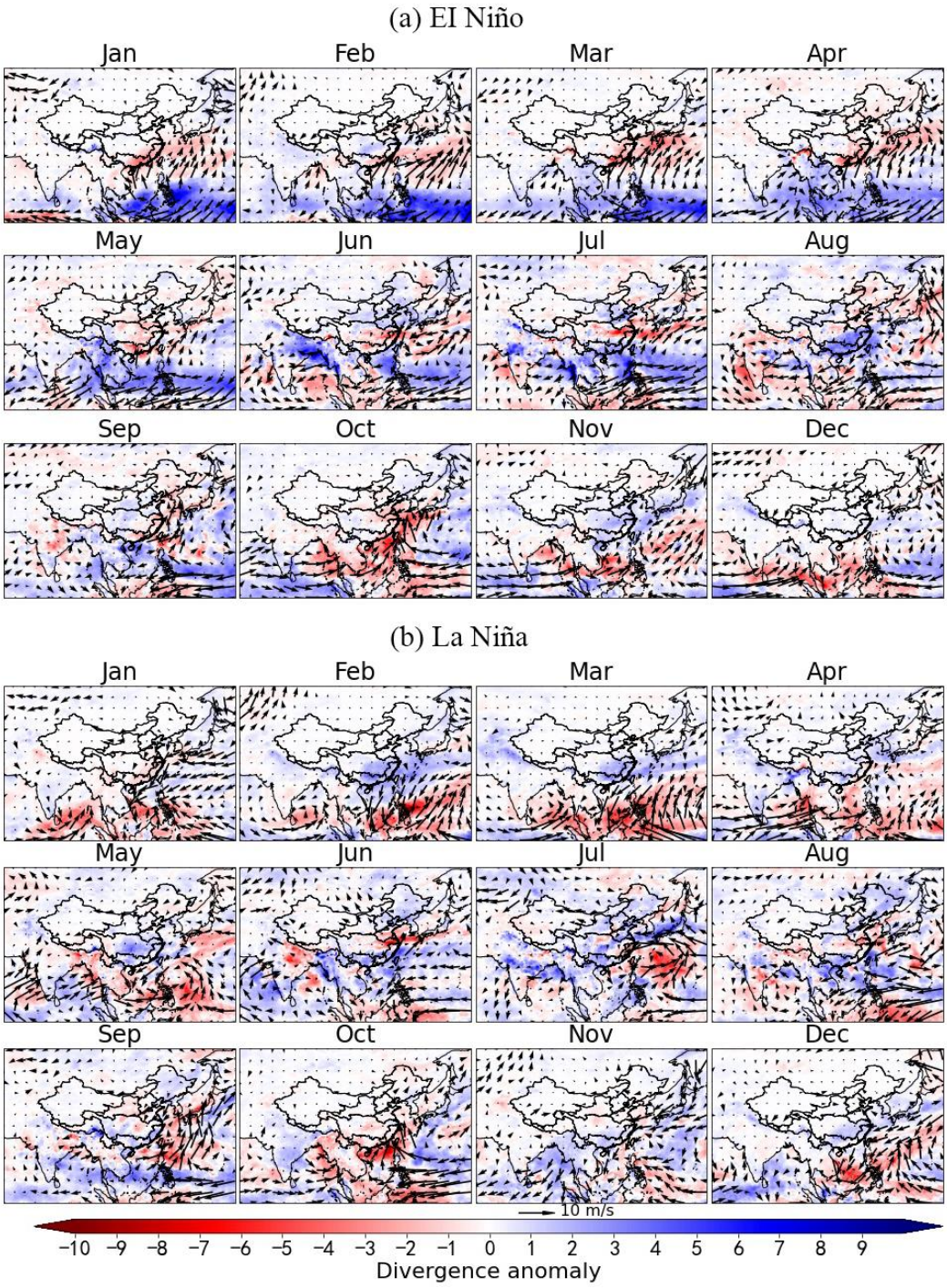

1101

1102 Figure 14 Monthly anomaly of vertical divergence (shading, unit: $kg \cdot m^{-2} \cdot s^{-1}$) in strong

1103 EI Niño and strong La Niña years from 1960 to 2018. The vector arrows indicate wind

1104 anomalies, and the direction indicates the direction of wind speed.

1105